

2009

Optimal micro heat pipe configuration on high performance heat spreaders

Seema Sandhaya Singh
San Jose State University

Follow this and additional works at: https://scholarworks.sjsu.edu/etd_theses

Recommended Citation

Singh, Seema Sandhaya, "Optimal micro heat pipe configuration on high performance heat spreaders" (2009). *Master's Theses*. 3683.
DOI: <https://doi.org/10.31979/etd.3mq6-m6aj>
https://scholarworks.sjsu.edu/etd_theses/3683

This Thesis is brought to you for free and open access by the Master's Theses and Graduate Research at SJSU ScholarWorks. It has been accepted for inclusion in Master's Theses by an authorized administrator of SJSU ScholarWorks. For more information, please contact scholarworks@sjsu.edu.

OPTIMAL MICRO HEAT PIPE CONFIGURATION
ON HIGH PERFORMANCE HEAT SPREADERS

A Thesis

Presented to

The Faculty of the Department of Mechanical and Aerospace Engineering

San José State University

In Partial Fulfillment

of the Requirements for the Degree

Master of Science in Mechanical Engineering

by

Seema Sandhaya Singh

May 2009

UMI Number: 1470973

INFORMATION TO USERS

The quality of this reproduction is dependent upon the quality of the copy submitted. Broken or indistinct print, colored or poor quality illustrations and photographs, print bleed-through, substandard margins, and improper alignment can adversely affect reproduction.

In the unlikely event that the author did not send a complete manuscript and there are missing pages, these will be noted. Also, if unauthorized copyright material had to be removed, a note will indicate the deletion.



UMI Microform 1470973

Copyright 2009 by ProQuest LLC

All rights reserved. This microform edition is protected against unauthorized copying under Title 17, United States Code.

ProQuest LLC
789 East Eisenhower Parkway
P.O. Box 1346
Ann Arbor, MI 48106-1346

© 2009

Seema S. Singh

ALL RIGHTS RESERVED

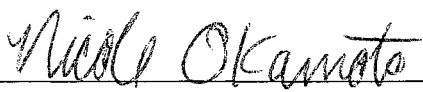
SAN JOSÉ STATE UNIVERSITY

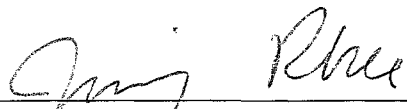
The Undersigned Thesis Committee Approves the Thesis Titled

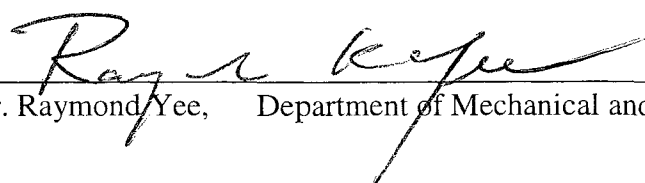
OPTIMAL MICRO HEAT PIPE CONFIGURATION
ON HIGH PERFORMANCE HEAT SPREADERS

by
Seema Sandhaya Singh

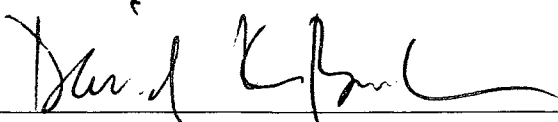
APPROVED FOR THE DEPARTMENT OF
MECHANICAL AND AEROSPACE ENGINEERING


Dr. Nicole Okamoto, Department of Mechanical and Aerospace Engineering Date 4/2/09


Dr. Jinny Rhee, Department of Mechanical and Aerospace Engineering Date 4/2/09


Dr. Raymond Yee, Department of Mechanical and Aerospace Engineering Date 4/2/09

APPROVED FOR THE UNIVERSITY


Associate Dean Date 4/20/09

ABSTRACT

OPTIMAL MICRO HEAT PIPE CONFIGURATION ON HIGH PERFORMANCE HEAT SPREADERS

by Seema S. Singh

The purpose of this research was to determine the optimal micro heat pipe (MHP) configuration on high performance heat spreaders. The ultimate goal was to reduce the spreading resistance and eliminate localized hot spots. Hot spots occur when the temperature is not evenly distributed throughout an area. To reduce these hot spots, an array of micro heat pipes was implemented into the heat spreader. Seven array configurations, ranging from 2 MHPs to 8 MHPs, were evaluated for a range of power inputs varying from 3 W to 21 W. The finite element software, MECHANICA 4.0, was utilized for the simulations. Through a comprehensive literature review, it was determined that evaluating the MHP limitations and finding an effective thermal conductivity were beyond the scope of this research. Therefore, a simplified equation was used for the MHP limitations, and the simulations were carried out for conductivities of 5,000 W/m°C, 50,000 W/m°C, and 100,000 W/m°C. The convective boundary condition was also varied to determine its effect on spreading resistance.

It was determined that the spreading resistance was independent of the convection coefficient and power input for a specific MHP effective thermal conductivity. The spreading resistance decreased with increasing effective thermal conductivities until the conductivity reached about 50,000 W/m°C, at which point the spreading resistance leveled off. The spreading resistance was found to decrease with increasing numbers of MHPs in the array. Overall, MHPs did aid in decreasing the spreading resistance.

ACKNOWLEDGEMENTS

This thesis could not have been completed without the aid of my committee members, most especially my committee chair, Dr. Nicole Okamoto. Her guidance throughout the research period, patience, and willingness to do what she could to aid in the timely completion of this thesis is most appreciated.

I'd also like to thank Dr. Eduardo Chan for his expertise in MECHANICA and for answering all my simulation-related questions.

Finally, I cannot continue without thanking Ms. Karishma Singh for all her assistance, not only in the completion of this thesis, but for her continual support throughout my academic studies.

Table of Contents

List of Figures.....	viii
List of Tables.....	ix
Nomenclature.....	x
1 Introduction.....	1
2 Objectives and Methods	3
3 Literature Review	5
3.1 Spreading Resistance	5
3.2 Heat Pipes	7
3.2.1 Operation	7
3.2.2 Construction.....	8
3.2.3 Advantages	9
3.2.4 Limitations.....	9
3.3 Micro Heat Pipes	11
3.3.1 Overview.....	11
3.3.2 Limitations.....	12
3.3.3 Cross-Sectional Area	14
3.3.4 Orientation and Quantity	15
3.3.5 Effective Thermal Conductivity	17
4 Benchmark.....	18
4.1 Benchmark Model Setup	19
4.2 Benchmark Results and Discussion.....	24
4.3 Convergence and Accuracy in the Solution.....	27
5 Array Configurations.....	30
5.1 Model Setup.....	30
5.1.1 Engineering Equation Solver (EES)	30
5.1.2 MECHANICA	33
5.2 Results and Discussion	38
5.2.1 Surface Temperatures and Power Input.....	38
5.2.2 Array Configuration and Effective Thermal Conductivity.....	40
5.2.3 Convection Boundary Condition	44
5.2.4 Pattern Radius	45

5.2.5 Diamond Heat Spreader	46
6 Conclusions and Recommendations	49
Works Cited	53
Appendix	55
EES Formula Sheet	55
Array Configurations	56

List of Figures

Fig. 1: The radial MHP configuration to be studied.....	3
Fig. 2: Heat pipe operation.	8
Fig. 3: Star and rhombus MHPs.	15
Fig. 4: Kang and Huang's experimental setup.....	19
Fig. 5: Settings selections in AutoGem.	21
Fig. 6: Shape and dimensions of the benchmark MHP.	22
Fig. 7: The 4 in x 4 in silicon wafer with embedded MHPs.....	23
Fig. 8: Plot of maximum temperature vs. power input.	25
Fig. 9: Plot of effective thermal conductivity vs. power input.	26
Fig. 10: Maximum temperature and effective thermal conductivity.	27
Fig. 11: Cross-sectional area of the MHP.....	31
Fig. 12: Power inputs as a function of the quantity of MHPs.....	33
Fig. 13: Temperature measures.....	35
Fig. 14: Surface temperatures as a function of power input.	39
Fig. 15: Average and maximum spreading resistance as a function of power.	40
Fig. 16: Average and maximum spreading resistance as function of the quantity of MHPs.	40
Fig. 17: Average and maximum spreading resistance as a function of effective thermal conductivity.	42
Fig. 18: Average and maximum spreading resistance for a range of effective thermal conductivities.	43
Fig. 19: Average and maximum spreading resistance.	45
Fig. 20: Pattern radius.....	46
Fig. 21: Spreading resistance of three different types of diamond spreaders, all compared to MHP Array 8.	48
Fig. 22: Array 3 patterned around the heat source with a radius of 4.25 mm.	52

List of Tables

Table 1: MECHANICA options used to complete the benchmark study.....	20
Table 2: Parameters defined in the MECHANICA simulations.....	37
Table 3: Temperature and spreading resistance.....	39
Table 4: Spreading resistance percent decrease from 2 MHPs to 8 MHPs.	42
Table 5: Results of pattern radius for Array 4 at $h=100\text{W/m}^2\text{C}$ and $k_{\text{eff}}=100,000$ W/m°C.....	46
Table 6: Spreading resistance comparison between no MHPs and with an array of 8 MHPs.	50

Nomenclature

A	cross sectional area, m
avg	average
b	plate radius, m
Bi	Biot number = hb/k
cf	correction factor
CVD	chemical vapor deposition
d	source radius, m
D_h	hydraulic diameter, m
h	heat transfer coefficient, $W/m^2\text{°C}$
h_{fg}	latent heat of vaporization, J/kg
k	thermal conductivity, $W/m\text{°C}$
K	shape factor
k_{eff}	effective thermal conductivity for MHPs, $W/m\text{°C}$
L	length, m
L_{eff}	effective length, m
q	heat flux, W/m^2
Q_{in}	heat input to evaporator, W
\dot{Q}_{max}	maximum power, W
R_{avg}	average thermal resistance, °C/W
r_{ca}	capillary radius, m
r_h	hydraulic radius, m
r_i	radius of the inner heat pipe wall, m
R_{max}	maximum thermal resistance, °C/W
r_n	nucleate site radius, m
R_{sp}	thermal spreading resistance, °C/W
t	thickness of spreader plate, m
T	temperature, °C
\bar{T}_{base}	average base temperature, °C
T_{max}	maximum base temperature, °C
\bar{T}_{source}	average source temperature, °C

Greek Symbols

β	liquid shape parameter
ε	dimensionless contact radius, d/b
λ	dimensionless parameter
ν	kinematic viscosity, m^2/s
ρ	density of fluid, kg/m^3
σ	surface tension, N/m
τ	dimensionless plate thickness, t/b
ϕ	dimensionless parameter
ψ	dimensionless constriction resistance
Δp	change in pressure, N/m^2

Subscripts

a	adiabatic
ax	axial
b	boiling
c	condenser
ca	capillary
e	evaporator
l	liquid
max	maximum
n	normal hydrostatic
v	vapor

1 Introduction

The motivation for this research comes from a specific engineering problem seen in industry today. Rockwell Collins, a communications and aviation electronics solutions company, presented a cooling situation involving a heads-up display for military cockpits. The heads-up display allows the pilot to keep looking straight ahead instead of down when observing crucial flight markers. In the Rockwell Collins situation, conventional military cockpit displays are replaced with indicator lights known as Light Emitting Diodes or LEDs (Okamoto, Personal Interview). LEDs are becoming increasingly popular because they produce more light per watt than incandescent bulbs in a smaller footprint, saving space, energy, and money. They are also ideal for situations where there is frequent on/off cycling. Hence, using LEDs is a sensible solution for military cockpits.

However, the recent trend of minimizing the size of electronic products, such as using LEDs, poses a challenge in thermal engineering. As the heat source gets smaller, the power density increases. This creates an issue on how to effectively remove heat from the heat source and how to effectively decrease the spreading resistance. Spreading resistance occurs when heat flows from a smaller surface area to a larger surface area, such as from a small heat source to a larger heat sink. Adequate heat removal is an extremely important issue to address because it affects component performance, life, and reliability.

In the Rockwell Collins example, an array of 9 x 9 LEDs are placed together, dissipating power in a 9 mm x 9 mm area. Each array produces 45 W of power and is

attached to a 2 inch x 2 inch heat spreader. This results in an extremely high power density and makes it difficult to adequately remove heat, especially at altitudes of up to 25,000 feet where air for convection cooling is minimal. Such a high concentration of heat also creates numerous problems with spreading resistance. Therefore, other methods of cooling must be utilized to decrease the spreading resistance.

The most current solution proposed, applied to the Rockwell Collins' problem, was to use synthetic diamond as a heat spreader between the concentrated LED array to the heatsink base. Although this proved to be an exceptional way to decrease the spreading resistance, it was too expensive to be plausible. As a result, cost-effective solutions were proposed. It was determined from preliminary calculations that a copper substrate with embedded micro heat pipes would be comparable to the diamond spreader in thermal performance, and would result in a much cheaper thermal package (Okamoto, Rhee, Lee, and Gleixner).

2 Objectives and Methods

The objective of this research was to find the optimal MHP configuration embedded in a copper heat spreader that would significantly reduce the spreading resistance. The goal was to introduce a procedure and document trends on how different parameters affect the spreading resistance. Arrays with increasing numbers of MHPs were examined. In each array configuration, the angle between the MHPs was equally spaced as shown for an array of eight MHPs in Fig. 1. As the number of MHPs changed, the angle changed as well. To determine the most effective MHP configuration, finite element analysis was performed using MECHANICA 4.0 software.

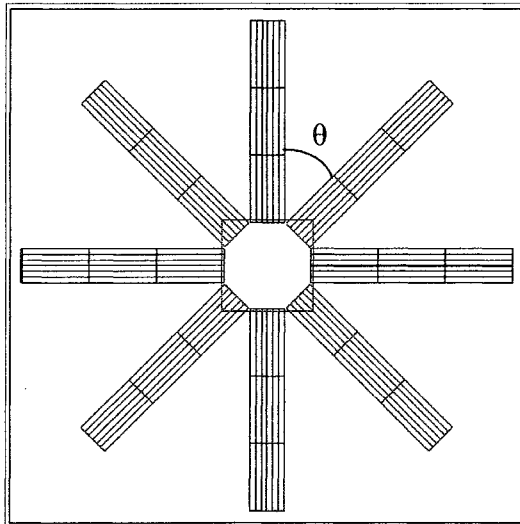


Fig. 1: The radial MHP configuration to be studied.
The angle θ was varied along with the number of MHPs.

Before any simulations were conducted, a literature review was completed examining heat pipes and spreading resistance in general, followed by a more extensive review on MHPs. In particular, typical MHP diameters and lengths, effective thermal

conductivities, and MHP limitations were all examined. A benchmark of a current heat pipe configuration was completed to validate the use of MECHANICA for an array of MHPs. Simulations were conducted for several MHP geometries. Each MHP in the model was assigned a typical effective thermal conductivity that was determined from the literature review, and different boundary conditions were applied. The inner workings of the MHP, including evaporation and condensation, were not modeled due to the scope of this research. Data were presented in terms of spreading resistance with respect to various parameters, such as the number of MHPs and boundary conditions. The range of power inputs modeled was found in the literature review and through preliminary simulations. Plots of the different trends were presented along with general recommendations outlining the most effective MHP configuration that most effectively reduced the spreading resistance.

3 Literature Review

3.1 Spreading Resistance

Spreading resistance occurs when there is a change in cross-sectional area, particularly when a large area is used to spread the heat from a small heat source. As electronic devices and components continue to shrink, the spreading resistance becomes an increasingly important issue. In electronics packaging, it is typically in the form of the small heat source connected to the base of a larger heat sink. The heat spreads across the heat sink base such that there is a much higher heat flux near the source in the middle of the heat sink than there is at the outer edges of the heat sink base. As a result, the heat sink is not able work as efficiently as it could if the heat had been spread uniformly across the heat sink base. Thus, the spreading resistance is an extremely important subject matter to address, and one must understand what factors affect it before any progress is be made to decrease it.

In their research, Lee, Song, Au, and Moran discuss how the spreading resistance is calculated from the geometry and size of the heat source and spreader plate. The source and spreader radius, d and b , are determined from the source and spreader areas by using Equation 1 and Equation 2, respectively. The equations are valid for a square heat source that is centered on a square base plate.

$$d = \sqrt{\frac{A_s}{\pi}} \quad (1)$$

$$b = \sqrt{\frac{A_p}{\pi}} \quad (2)$$

The spreading resistance is then calculated from the resulting radii using Equations 3 to 9. It is shown that the spreading resistance is a function of the ratio of the effective radii, d and b , the thickness of the spreader plate, t , the thermal conductivity of the spreader plate, k , and the heat transfer coefficient, h .

$$\varepsilon = \frac{d}{b} \quad (3)$$

$$\tau = \frac{t}{b} \quad (4)$$

$$Bi = \frac{h \cdot b}{k} \quad (5)$$

$$\lambda = \pi + \frac{1}{\varepsilon \sqrt{\pi}} \quad (6)$$

$$\phi = \frac{\tanh(\lambda \cdot \tau) + \frac{\lambda}{Bi}}{1 + \frac{\lambda}{Bi} \tanh(\lambda \cdot \tau)} \quad (7)$$

$$\psi_{\max} = \frac{\varepsilon \cdot \tau}{\sqrt{\pi}} + \frac{1}{\sqrt{\pi}} (1 - \varepsilon) \phi \quad (8)$$

$$R_{sp} = \frac{\psi_{\max}}{k \cdot d \cdot \sqrt{\pi}} \quad (9)$$

While Lee, Song, Au, and Moran sought to determine the spreading resistance in terms of the heat source and spreader geometry, Song, Lee, and Au developed simplified

equations for finding the spreading resistance where the base of the spreader plate is not isothermal but instead exposed to a uniform heat transfer coefficient. Here the thermal spreading resistance is defined by temperatures and the rate of heat transfer. The average thermal spreading resistance is shown by Equation 10, and the maximum thermal spreading resistance is shown by Equation 11, where \bar{T}_{source} is the average source temperature, \bar{T}_{base} is the average base temperature on the opposite side of the heat source, T_{max} is the maximum temperature at the heat source, and \dot{Q} is the rate of heat transfer. These resistances take into account both the spreading resistance and the bulk material resistance from the plate thickness.

$$R_{avg} = \frac{\bar{T}_{source} - \bar{T}_{base}}{\dot{Q}} \quad (10)$$

$$R_{max} = \frac{T_{max} - \bar{T}_{base}}{\dot{Q}} \quad (11)$$

3.2 Heat Pipes

3.2.1 Operation

Heat pipes are hollow tubes made of a thermally conductive material. The inside of the tube consists of a wick and the liquid and vapor forms of a working fluid. Heat pipes operate on the principle of latent heat in the form of an internal evaporator and condenser on the two ends. As shown in Fig. 2, heat enters the evaporator section from the heat source where the liquid changes phase and turns into vapor. The vapor travels up to the condenser section of the pipe. The vapor condenses into a liquid as it releases heat energy and employs capillary pressure from the wick to travel back down to the

evaporator. Thus, the cycle continues by continuously removing heat away from the heat source.

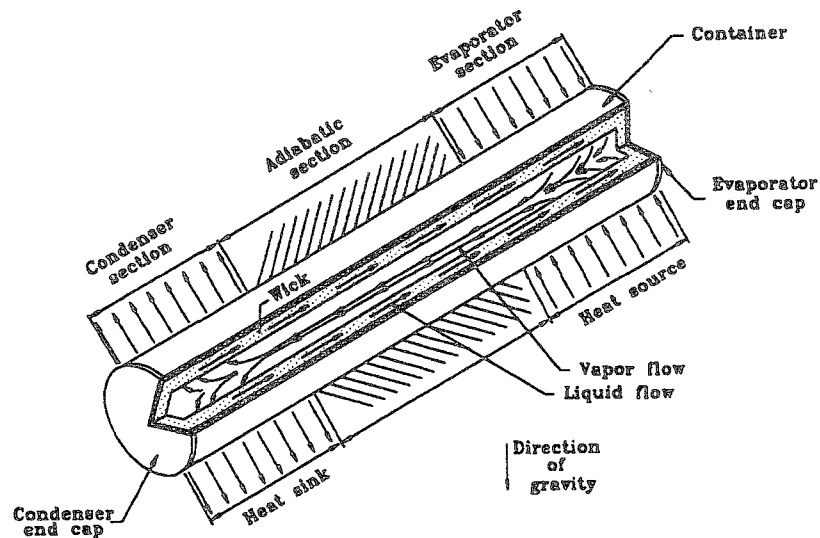


Fig. 2: Heat pipe operation.

Heat enters the evaporator portion and travels to the condenser as a vapor where it is dissipated by a phase change. The condensed liquid travels back to the evaporator by the wick and the cycle continues (Faghri 4). Reprinted with permission.

Heat pipes are extremely efficient components that rapidly transport large heat fluxes away from a heat source and are used in situations that have a relatively small temperature difference between the two ends of the heat pipe. The evaporator and condenser are isothermal in nature, meaning that they keep a constant temperature for small variations in power input. This constant temperature is at the saturation temperature at a specified heat-pipe pressure.

3.2.2 Construction

Heat pipes are simple devices with simple construction. The outer portion of the heat pipe is made from a thermally conductive material, such as copper or aluminum.

Inside the tube is a wick that uses capillary pressure to transfer the liquid back to the evaporator. The wick can be grooves in the pipe, fine fiber, a screen mesh, or sintered metal (McCloskey). The fluid inside the heat pipe, the working fluid, varies as well and depends on the heat source temperature and the application for which it is being used. For most cases, such as in electronic equipment, water, ethanol or ammonia is used. The working fluid must be chosen carefully. In general, the fluid should be in the liquid phase at the cooler end of the heat pipe and in the vapor phase at the hotter end of the pipe and must be compatible with the outer heat pipe material.

3.2.3 Advantages

There are many advantages of using heat pipes. Heat pipes have no moving parts, so they are quiet, require virtually no maintenance and are highly reliable. They do not require an external power source other than the heat source itself to operate. They are relatively small in size and weight, making them desirable components for cooling small devices. Heat pipes have “precise isothermal control” so that the input heat fluxes can vary without large changes in the operating temperature (Yeh and Chu). They also work in any orientation.

3.2.4 Limitations

Although heat pipes are very beneficial, there are many limits that must be acknowledged before they can be implemented. For one, the capillary pressure must be great enough to wick the liquid back to the evaporator. The capillary pressure between the condenser and the evaporator must be greater than the sum of the pressure drops due

to the normal hydrostatic pressure, the axial pressure, the viscous liquid pressure, and the viscous vapor pressure as shown in Equation 12 (Yeh and Chu).

$$\Delta p_{ca} \geq \Delta p_n + \Delta p_{ax} + \Delta p_l + \Delta p_v \quad (12)$$

If the capillary pressure is too low, liquid cannot be brought back to the evaporator.

Hence, the evaporator has no liquid to evaporate and dryout occurs. Once dryout occurs, the heat pipe no longer functions properly.

Another important limitation is the boiling limit. The boiling limit is when boiling occurs in the wick causing the liquid in the wick to evaporate before it makes it to the evaporator, preventing the liquid from completing the cycle in the heat pipe (Yeh and Chu). This is caused by a radial instead of axial heat flux and causes dryout in the heat pipe. The maximum heat flux that can be used is found in Equation 13.

$$q_b = \frac{2\pi \cdot (0.5L_e + L_a + 0.5L_c) \cdot k_{eff} \cdot T_v \left(\frac{2\sigma}{r_n} - \Delta p_{ca} \right)}{h_{fg} \cdot \rho_v \cdot \ln\left(\frac{r_i}{r_n}\right)} \quad (13)$$

Other limitations such as the sonic, entrainment, and viscous vapor flow limits must also be observed. The sonic limit occurs when the vapor velocity in the evaporator reaches sonic speed. When the condenser temperature is lowered in normal heat pipe operation, the evaporator temperature is lowered which increases the heat transfer rate. However, when the sonic limit is reached the vapor flow gets choked so the evaporator temperature is not affected when the condenser temperature is lowered (Yeh and Chu). Entrainment occurs when the vapor velocity is high enough that some of the liquid in the wick gets picked up in the vapor flow. Not enough liquid is carried to the evaporator which leads to dryout (Yeh and Chu). The viscous vapor flow limit occurs at a low heat

pipe operating temperature when the viscous forces prevent vapor flow from going to the condenser; the vapor pressure difference between the evaporator and condenser cannot overcome the viscous forces (Yeh and Chu).

3.3 Micro Heat Pipes

3.3.1 Overview

A literature review was conducted to find the best way to design the heat pipe model taking into account the specifications of the project and limitations of MHPs. Several factors had to be considered such as the shape, diameter, length, and orientation of the MHP before simulations could be conducted. All the factors had to be analyzed to determine if a MHP array could effectively distribute the heat that a LED array dissipates.

Over the years, numerous studies have been completed to analyze MHPs and their operation. MHPs used to cool microelectronic devices were first introduced by Cotter in 1984 who defined a micro heat pipe “as one so small that the mean curvature of the vapor liquid interface is necessarily comparable in magnitude to the reciprocal of the hydraulic radius of the total flow channel.” This is shown in Equation 14 where r_{ca} is the capillary radius and r_h is the hydraulic radius of the MHP.

$$\frac{r_{ca}}{r_h} \geq 1 \quad (14)$$

MHPs are approximately 100-1000 μm in hydraulic diameter and about 10-20 mm in length (Yeh and Chu). They operate in a similar manner to regular heat pipes. The main

difference is that MHPs don't have a wicking material. Instead, they have sharp corners that create the capillary pressure.

3.3.2 Limitations

MHPs are extremely sensitive to the operation limitations because of their small size, so care must be taken when designing them. Li *et al.* studied the heat transfer performance of small heat pipes and found that the entrainment factor for the capillary limit is more of a factor for heat pipes with a smaller diameter (Cao and Faghri). Cao and Faghri found that as the heat pipe size decreases, the vapor continuum limitation becomes more important for lower temperature heat pipes. The vapor continuum limit is a complicated phenomena involving "rarefied or free molecular flow resulting in a large temperature gradient along the heat pipe length" (Cao and Faghri 268). Even the amount of working fluid is important in MHPs. Too much working fluid can flood the heat pipe and too little can easily cause dryout.

Numerous articles have summarized that in most heat pipe applications the capillary pressure is the determining limit in MHP operation, no matter what type of heat pipe you have. Cao, Gao, Beam, and Donovan found through their experiments with flat miniature heat pipes that the capillary heat transfer limit was always the dominating limit, and it was largely due to the working temperature. In their experiments, they gradually increased the power until dryout occurred. They found that when dryout occurred at the end of the evaporator section, part of the adiabatic section of the heat pipe started to perform as the evaporator. It then became difficult to measure how much of the MHP was acting as the evaporator (Ha and Peterson). To find the maximum power, Ha and

Peterson proposed a semi-empirical correlation using Cotter's and Babin, Peterson, Wu's data as shown in Equation 15.

$$\dot{Q}_{\max} = cf \frac{0.16\beta\sqrt{K_l K_v}}{8\pi(0.5L_e + L_a + 0.5L_c)} \frac{\sigma h_{fg}}{\nu_l} \sqrt{\frac{\nu_l}{\nu_v}} A^{3/2} \quad (15)$$

Equation 15 is a function of several variables: the liquid shape parameter, β , the dimensionless liquid and vapor shape factors, K_l and K_v , the surface tension, σ , the latent heat of vaporization, h_{fg} , the liquid and vapor kinematic viscosities, ν_l and ν_v , the cross-sectional area, A , and the lengths of the evaporator, adiabatic and condenser sections, L_e , L_a and L_c , respectively. The entire equation is multiplied by a correction factor, cf , which for a copper-water heat pipe is 0.33, according to Babin, Peterson, and Wu. Equation 15 requires in depth coverage of the MHP, including analysis of the radius of curvature in the intrinsic meniscus, the local mass flow rates, half groove angles and several other involved variables and equations. Comprehensive analysis of the physics of MHP operation and limits is beyond the scope of this project but still extremely important. Therefore, it is suggested that detailed MHP analysis be completed to add to this research. To make calculations simpler and tie back into what this research entails, the maximum power equation proposed by Cao and Faghri is used. Shown by Equation 16, the maximum power is a function of only the liquid surface tension, the latent heat of evaporation, the hydraulic diameter, the vapor kinematic viscosity, and the total length of the MHP.

$$\dot{Q}_{\max} = 0.01 \frac{\sigma h_{fg} D_h^3}{\nu_v L} \quad (16)$$

By using Equation 16, the heat transfer limit is found fairly easily. Given the power to be dissipated from the LED array, a specific MHP length is calculated by changing the hydraulic diameter. The working fluid is easily changed by changing the liquid surface tension, latent heat of evaporation, and kinematic viscosity. By experimenting with the variables, an acceptable MHP diameter and length is found that fits onto the heat spreader.

3.3.3 Cross-Sectional Area

The shape of the MHP can greatly affect the heat transfer capacity. As mentioned before, MHPs have sharp corners in their design to create adequate capillary pressure. Common MHPs have rectangular or triangular cross-sections. Peterson, Duncan, and Weichold investigated arrays of MHPs in silicon wafers. They analyzed machined, rectangular channels 45 μm wide and 80 μm deep and etched, triangular channels 120 μm wide and 80 μm deep. Both heat pipe arrays reduced the maximum wafer temperature and intensity of localized hot spots. However, the triangular cross section MHP outperformed the rectangular one. The rectangular MHPs resulted in an effective thermal conductivity 31 percent greater than with no heat pipes, while the triangular heat pipes resulted in an effective thermal conductivity of 81 percent greater than with no heat pipes. The authors concluded that because the machined rectangular channels had more rounded corners, the capillary pumping pressure decreased, thus lowering the heat

transfer rate. The authors also mentioned that the machined MHPs also had scaly deposits which may also have contributed to the low heat transfer rate.

Similar results were also obtained by Suman, De, and DasGupta. The authors also tested triangular and rectangular MHPs, but their model was valid for any polygon shape. It was found that the MHP's sharper corners (smaller angle between the two adjacent sides) resulted in a greater capillary pumping pressure. Therefore, the triangular MHP with angles of 60 degrees each had a greater capillary pressure than a rectangle with angles of 90 degrees each.

Kang and Huang conducted a similar experiment with star and rhombus shaped MHPs as shown in Fig. 3. Both designs have sharp, acute angles and micro gaps that aid in capillary pressure. It was found that the effective thermal conductivity was over 34 percent better for the star and rhombus cross sections when compared to the triangular cross-sections.

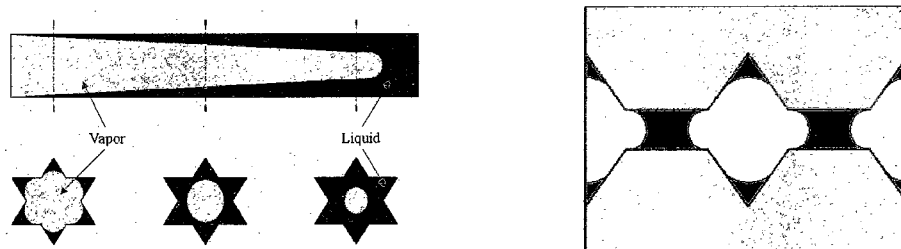


Fig. 3: Star and rhombus MHPs.
MHPs with a star (left) and rhombus (right) cross-sectional area as shown in Kang and Huang. Reprinted with permission.

3.3.4 Orientation and Quantity

Suman, De, and DasGupta tested MHPs with rectangular and triangular cross-sectional areas at different inclination angles and found that the tilt angle cannot be

ignored. Gravity affected the dryout and capillary limits of MHPs. The greater the tilt angle, the faster the capillary limit was reached. This means greater inclination angles increased the time at which the critical heat input limit was reached. It was assumed that the condenser was at a lower position than the evaporator. Similarly, in their experiments, Cao, Gao, Beam, and Donovan found that placing the heat pipe in a vertical orientation with the evaporator at the bottom greatly enhanced the heat transfer because of the reflux working conditions of the heat pipe.

The orientation of a heat pipe refers to the way heat pipes are positioned with respect to gravity. If the heat pipe is positioned such that the evaporator portion is lower than the condenser portion, the vapor rises and gravity assists the wick in bringing the liquid down the heat pipe. A heat pipe oriented this way is “gravity assisted”. When placing heat pipes, one must always make sure that they are oriented favorably with respect to gravity. Since gravity effects were disregarded in this research, all MHPs were oriented the same way by placing them all horizontally.

The quantity of heat pipes was also analyzed. Mallik, Peterson, and Weichold used heat pipes as part of semiconductor devices. They varied the number of heat pipes and found that increasing the number of heat pipes greatly reduced the maximum chip temperature. However, at 19 heat pipes, the percentage of temperature reduction reduced significantly in their setup. Thus, in their setup, there was no reason to add additional heat pipes at this point; the increase in thermal performance starts to slow down. The maximum number of MHPs varies for different setups depending on the MHP geometry and the heat flux applied.

3.3.5 Effective Thermal Conductivity

Because heat pipes utilize latent heat, they have extremely high effective thermal conductivities. Therefore, when modeling a heat pipe as a solid rod in simulation studies, an effective thermal conductivity, k_{eff} , must be used. Sobhan and Peterson presented this effective thermal conductivity as shown in Equation 17, where Q_{in} is the heat input to the evaporator section, A is the overall cross-sectional area of the heat pipe, T_e and T_c are the temperatures at the evaporator and condenser ends of the heat pipe, respectively, and L is the total length of the heat pipe.

$$k_{eff} = \frac{Q_{in}}{A \left[\frac{T_e - T_c}{L} \right]} \quad (17)$$

From the equation, it's seen that k_{eff} must be re-evaluated each time the heat input is changed. To get an accurate value of the effective thermal conductivity, a detailed analysis must be conducted regarding the inner workings of the MHP, such as the liquid charge, contact angles and shear stresses. However, that was beyond the scope of this research. Instead, a suggested value of 50,000 W/m°C was used as an average value of k_{eff} (Thyrum). Effective thermal conductivities of 5,000 W/m°C and 100,000 W/m°C were also tested for each array configuration to determine how the effective thermal conductivity affected the spreading resistance.

4 Benchmark

A benchmark was completed to validate the use of MECHANICA by comparing results with an existing paper. The paper utilized as the benchmark was Kang and Huang's "Fabrication of star grooves and rhombus grooves micro heat pipe". In this paper, the authors set up experiments measuring the maximum and minimum temperatures of a silicon wafer with 31 embedded star shaped MHPs. They did this for a range of power inputs. Fig. 4 shows the experimental setup. Power was supplied to the heater portion by a Topward 6303D power supply. K-type thermocouples were attached close to the evaporator and condenser areas of the wafer and was read by an Omega OMB-1100 data acquisition unit which was connected to a computer. Water kept at 19 ± 0.1 °C and regulated by a thermostat was used to cool the condenser portion of the MHP array. Although star and rhombus shaped MHPs were tested, only the star-shaped MHP experiment was used for this benchmark. The experiment was modeled in MECHANICA using an effective thermal conductivity for the MHPs. The goal was to obtain a similar trend to the that of Kang and Huang's experimental results.

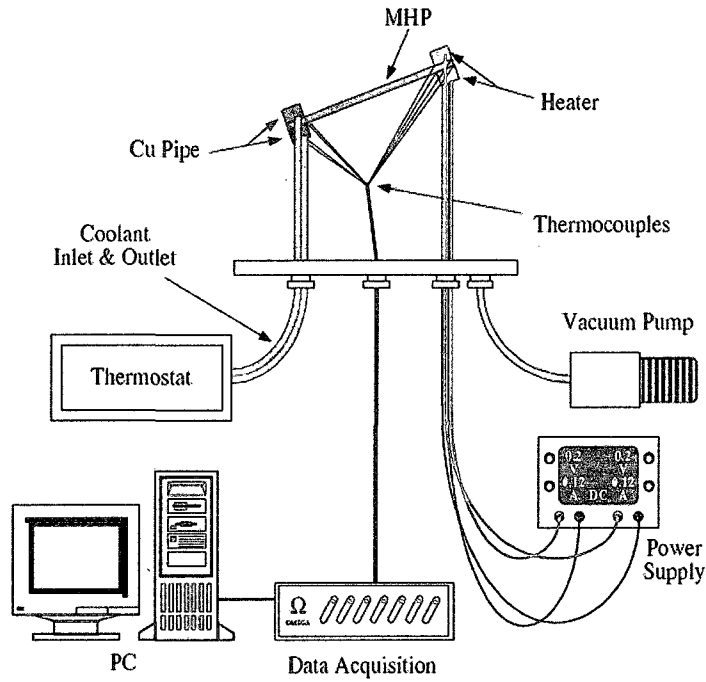


Fig. 4: Kang and Huang's experimental setup.
Reprinted with permission.

4.1 Benchmark Model Setup

The options and selections in MECHANICA used to complete the benchmark study are shown in Table 1. The integration mode allows for easy integration from Pro/Engineer, whereas in the independent mode, MECHANICA is independent of Pro/Engineer. The model is a 3D model with solid elements. There is an option of doing a steady-state or thermal analysis. For the present work, only the steady-state case is evaluated. There are a few options for convergence methods. One is the quick check method where the model is run at a low polynomial order and should only be used as an initial review of possible errors in the model. The single pass adaptive (SPA) performs only one pass, meaning that MECHANICA only fixes the problem elements once using

an edge order it thinks accurate. The multi-pass adaptive (MPA), which is the convergence method used in this study, increases the edge polynomial order until convergence or the maximum order is reached. For the benchmark study, the convergence was set to 10 percent on local temperature and local energy norms and was set to the 9th polynomial order. The mesh settings were monitored by AutoGEM. The AutoGEM settings used in the model are shown in Fig. 5. Most of the default values were used. However, due to the size and angles of the MHPs used in this study, the maximum edge turn had to be changed. The smallest MHP angle was 54.7 degrees so the edge turn was lowered to 50 degrees from the default value of 95 degrees to ensure that elements were created within the MHP.

Table 1: MECHANICA options used to complete the benchmark study.

	Options	Selection
Mode of Operation	Independent, Integrated	Integrated
Type of Model	3D, Plane Stress, Plane Strain, Axisymmetric	3D
Type of Element	Shell, Beam, Solid, Spring, Mass	Solid Elements
Analysis Method (Thermal Only)	Steady State, Transient	Steady State
Convergence Method	Quick Check, Single Pass Adaptive, Multi-Pass Adaptive	Multi-Pass Adaptive
Design Study	Standard, Sensitivity, Optimization	Standard

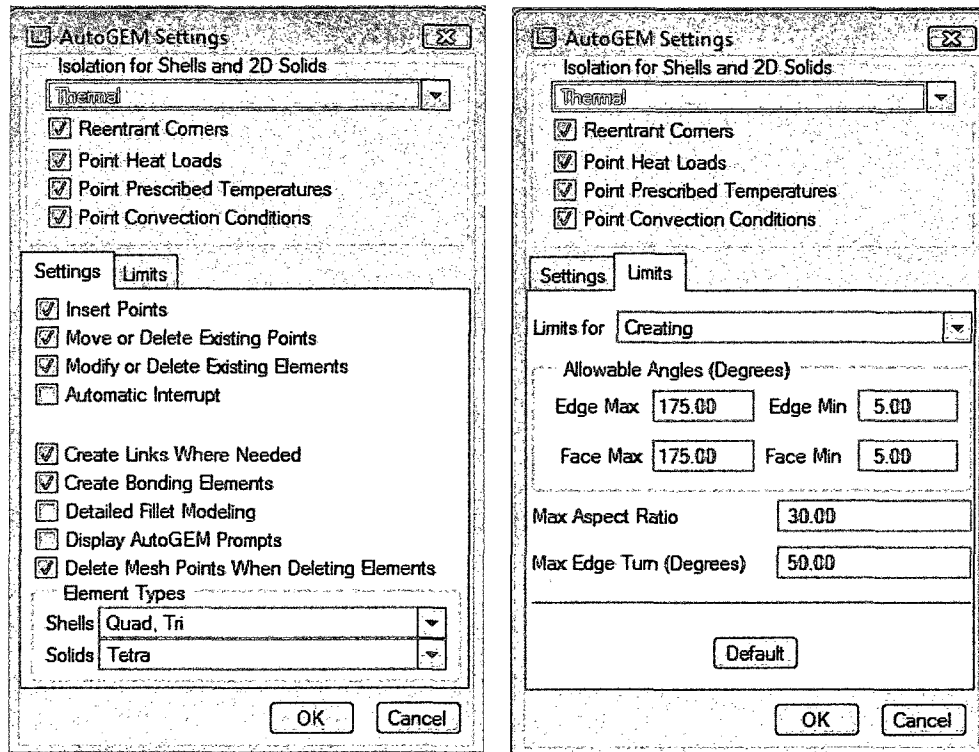


Fig. 5: Settings selections in AutoGem.

All settings are MECHANICA defaults except for the max edge turn which was set to a lower value of 50 degrees.

The star-shaped MHP was modeled with the cross section and dimensions shown in Fig. 6. Three parts were created and assembled together to simulate the three sections of the MHP. The evaporator and condenser lengths were 6 mm each, and the adiabatic length was 13.4 mm as obtained from Kang and Huang's paper. The 4 inch x 4 inch, 1.37 mm thick silicon wafer was then created with 31 cuts for each MHP. The MHPs were 0.820 mm apart and located in the center of the wafer occupying only a 25.4 mm x 25.4 mm area. The MHPs were then assembled into the wafer with a bonded interface. The bonded interface assured that heat was transferred through the different components.

An additional interface was created on the adiabatic section of the MHP such that there was no heat transfer from that portion of the MHP to the silicon wafer.

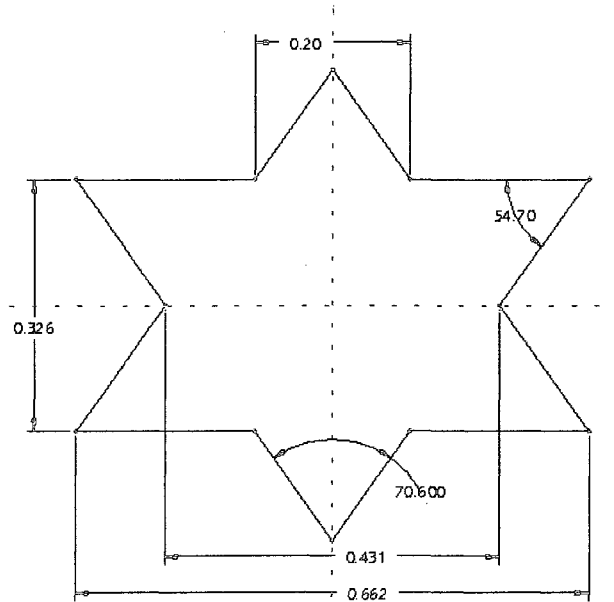


Fig. 6: Shape and dimensions of the benchmark MHP.
Length dimensions are in millimeters. Angle dimensions are in degrees.

The wafer was assigned the material silicon which had a thermal conductivity of $124 \text{ W/m}^\circ\text{C}$. The effective thermal conductivity of the MHPs was not stated in Kang and Huang's analysis and could not be backed out from the data given. Therefore, an estimated value of $100,000 \text{ W/m}^2^\circ\text{C}$ was assigned to each MHP. All surfaces of the wafer were adiabatic with the exception of the boundary conditions: the heat load applied and the convection condition. The input power was applied to the evaporator section of the MHP, and the convection boundary condition was applied to the condenser section. The power applied was varied from 0 W to 20 W as Kang and Huang did in their experiments. The boundary condition that was applied to the condenser portion of the silicon wafer could not be accurately found with the information given in the paper. It

was known that the area was being cooled by water at 19°C, but neither the velocity of the water nor the tube geometry were given, making the heat transfer coefficient impossible to calculate. It was assumed, however, that the heat transfer coefficient would be fairly high. Therefore, an estimated value of 1,000 W/m°C was used with a bulk temperature of 19°C. The boundary conditions were applied on the evaporator and condenser portions covering a 25.4 mm by 6 mm area as shown in Fig 7.

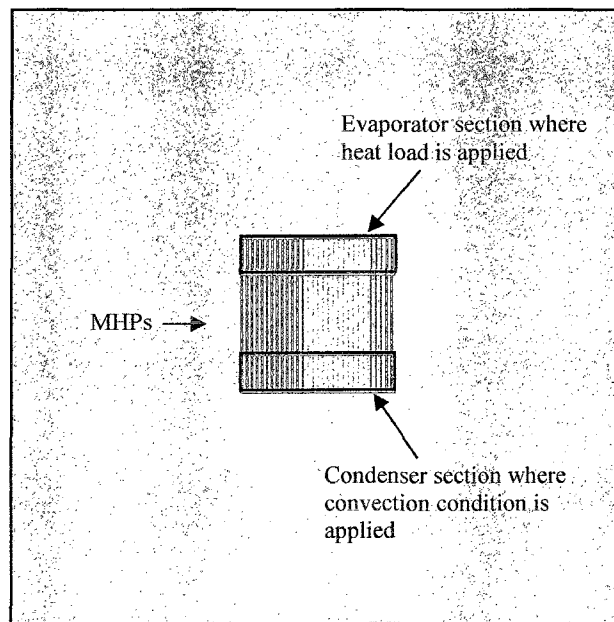


Fig. 7: The 4 in x 4 in silicon wafer with embedded MHPs.

The MHPs only occupy a 25.4 mm x 25.4 mm area. Each boundary condition is applied to a 24.5 mm x 6 mm area on the condenser and evaporator sections of the MHP.

The maximum and minimum temperatures at the evaporator and condenser were determined using MECHANICA. The maximum temperature was calculated as the average value of four temperature readings located 1.5 mm apart along the centerline that is 1 mm from the edge of the evaporator. The minimum temperature was calculated as the average value of four temperature readings located 1.5 mm apart along the centerline

that is 1 mm from the edge of the condenser. The maximum temperature was then plotted for each power input. The effective thermal conductivity of the silicon wafer was also plotted as a function of power. The formulas Kang and Huang used to calculate this conductivity is found in Equation 18, where L_{eff} is the effective length shown in Equation 19, and A_{eff} is the cross-sectional area of the wafer. L_{eff} had a value of 19.4 mm, and A_{eff} had a value of 70 mm². T_e and T_c were the average temperatures on the evaporator and condenser sides, respectively.

$$k_{eff, silicon} = \frac{Q_{in} \cdot L_{eff}}{A_{eff} (T_e - T_c)} \quad (18)$$

$$L_{eff} = L + \frac{L_e + L_c}{2} \quad (19)$$

It should be noted that since the convection boundary condition could not be calculated and the effective thermal conductivity of the MHPs was estimated, the results shown in Kang and Huang's paper could not be duplicated precisely. Instead, a successful benchmark was one in which the trends of the two plots presented were similar.

4.2 Benchmark Results and Discussion

The temperature versus power input plots obtained from the MECHANICA simulations were compared with those presented by Kang and Huang and are shown in Fig. 8. Although both plots are linear, the MECHANICA plot has a slope of 6.6 °C/W, and the paper result has a smaller slope of 5.05 °C/W. This could be due to the fact that the convection coefficient was too low. For a constant power input, cross sectional area, and ambient temperature, if the heat transfer coefficient is increased, the maximum surface temperature must decrease. Therefore, if a greater coefficient value was chosen,

the maximum temperatures would be lower and better match the values and slope presented by Kang and Huang.

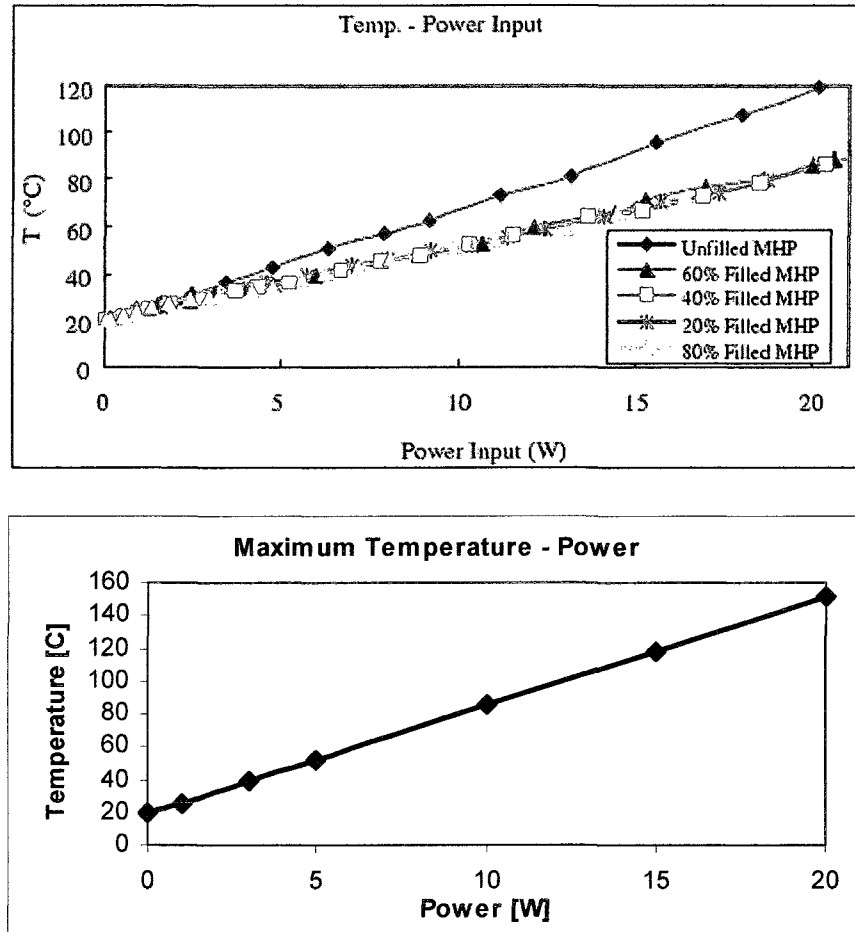


Fig. 8: Plot of maximum temperature vs. power input. Obtained from Kang and Huang (top) (reprinted with permission) and from the MECHANICA simulation (bottom). Both plots show a similar trend.

The effective thermal conductivity of the wafer as a function of power for both Kang and Huang's and the MECHANICA plots are shown in Fig. 9. Both plots show the same trend. In both plots, for higher power inputs, the effective thermal conductivity of the wafer is constant. It was expected that the thermal conductivity would stay constant

at higher power inputs because the power was directly proportional to the temperature difference between the evaporator and condenser sections of the wafer. This shows that at a constant effective length and area, as the power input increases the temperature difference must also increase in addition to the actual maximum temperature.

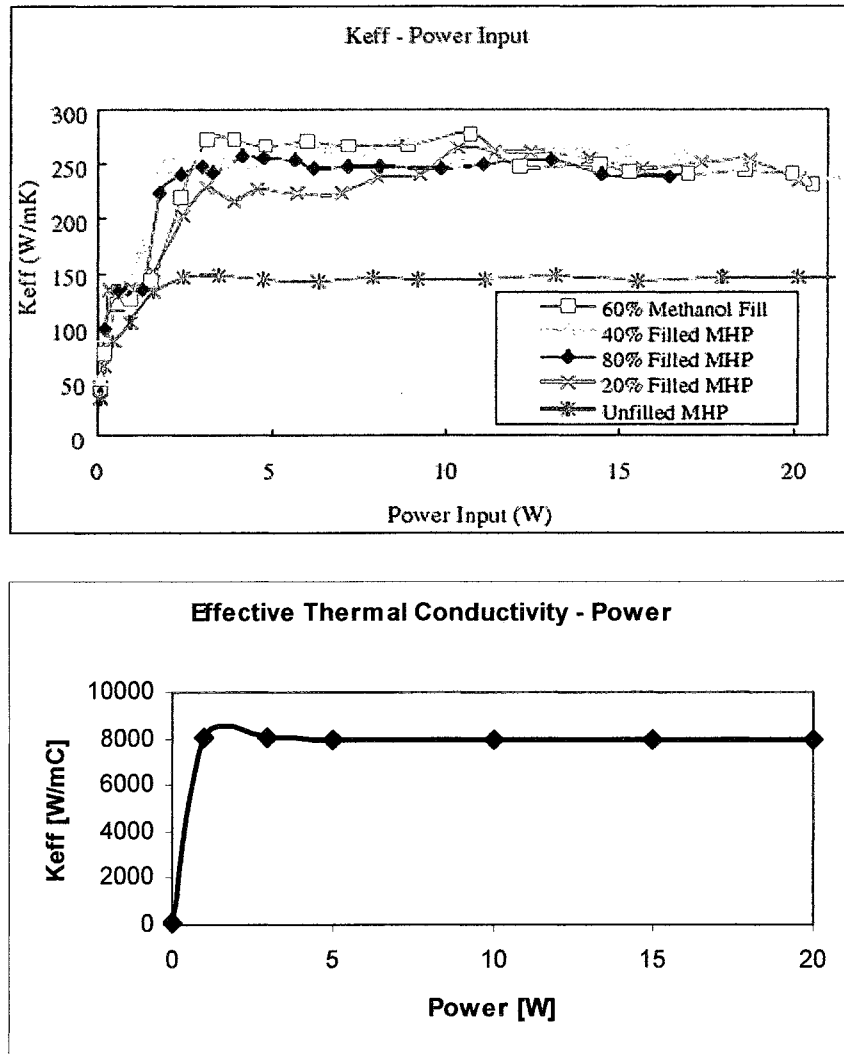


Fig. 9: Plot of effective thermal conductivity vs. power input. Obtained from Kang and Huang (top) (reprinted with permission) and from the MECHANICA simulation (bottom). Both plots show a similar trend.

Although not part of the benchmark procedure, it was interesting to examine the effect MHPs had on the maximum temperature and effective thermal conductivity of the wafer. To accomplish this a separate simulation was completed without any MHPs. The boundary conditions were applied to just the silicon wafer at the same location, and the temperatures were measured. The results are shown in Fig. 10. At higher power inputs the maximum surface temperature decreased with the addition of the MHP array. At 20 W the temperature decreased by as much as 44°C. The effective thermal conductivity of the wafer also improved with the addition of the MHP array. The conductivity increased from 117 W/m°C to 8000 W/m°C. Note that these results were from the MECHANICA simulation and did not reflect the exact physics of the problem. It was expected that there would be a maximum conductivity of the wafer close to that of the MHP where the conductivity could not get any higher with further addition of MHPs.

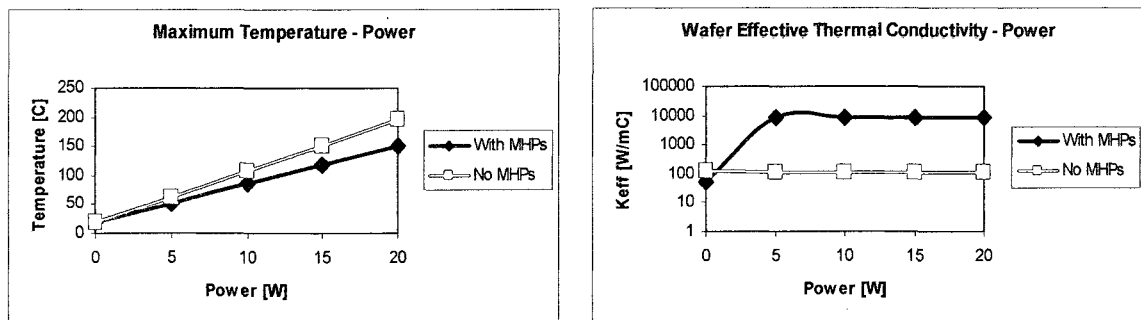


Fig. 10: Maximum temperature and effective thermal conductivity. Maximum temperature (left) and effective thermal conductivity (right) of the wafer as a function of power input.

4.3 Convergence and Accuracy in the Solution

When meshing a model two types of elements can be used, h-type or p-type. H-type elements always have a linear edge order regardless of the element shape. These

edges are derived and connected by Gaussian points. The h refers to the increment size. Larger increments result in more significant errors. The error is reduced by increasing the number of elements in the model using mesh refinement. One must keep refining the mesh until there are no significant changes in the solution, meaning that the solution has converged.

P-type elements, on the other hand, refer to the element edge polynomial order. Here, instead of increasing the number of elements to obtain convergence, the polynomial order on each element is increased while the mesh geometry stays the same; there is no need to increase the number of elements.

MECHANICA uses p-type elements in its calculations. If an element is in need of refinement, it is automatically bumped up to a higher order. However, not all elements are changed to a higher order. Only the elements that need refinement are increased. This process is continued until the solution reaches a value defined by the user. This selection is chosen by the AutoGEM and the Multi-Pass Adaptive options in MECHANICA under percent convergence. Mechanica increases the polynomial size up to a 9th order. Although it is rare, if the solution still does not converge with the 9th order, the mesh can be refined by increasing the number of elements. Because of MECHANICA's ability to automatically monitor convergence, it was not necessary to do a separate polynomial or grid analysis.

Although a grid or polynomial analysis was not needed, a convergence analysis was completed. In MECHANICA, the convergence percent could be set to a certain value. There were three options that values converge on: 1) local temperatures and local

energy norms, 2) local temperatures and local and global energy norms or 3) the measures the user specifies. The default value of converging on local temperatures and local energy norms was used for this study. The benchmark example was run at 30, 20, 10 and 5 percent convergence to determine how the maximum silicon surface temperature was affected.

From the results obtained, it was determined that the convergence value did not significantly change any of the temperature values. The difference between a 30% and 10% convergence was approximately 0.2%. Therefore, a 30% convergence value could be used to obtain accurate results. However, to save setup time, the default value of 10% converging on local temperature and local energy norms was used for this study. The default polynomial edge order of 6 was also used.

5 Array Configurations

5.1 Model Setup

5.1.1 Engineering Equation Solver (EES)

A 2 inch by 2 inch copper spreader characterized by a thermal conductivity of $400 \text{ W/m}^\circ\text{C}$, was subject to heat load centered on a 9 mm by 9 mm area. Star shaped MHPs with an effective thermal conductivity and with the cross-sectional area shown in Fig. 11.were placed around this heat source to decrease the spreading resistance. It was determined from the literature review that the capillary limit was one of the most important MHP limitations. To find this limit, Equation 16 was used and implemented into EES. EES was then utilized to experiment with, and to determine various parameters, such as the cross-sectional size of the heat pipe, the maximum power each heat pipe dissipated, the circular radius within the heat source area which the MHPs were patterned around, the maximum number of MHPs that could fit on the spreader, and the minimum number of MHPs needed to dissipate the total power. The formulas used in EES is found in the EES Formula Sheet in the Appendix.

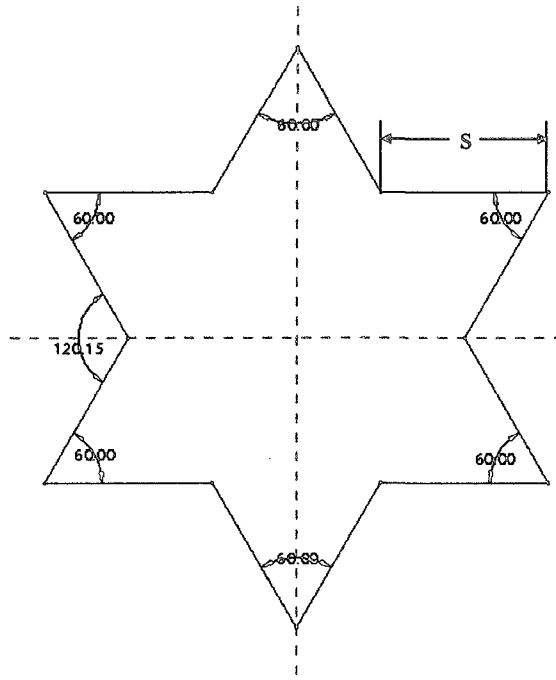


Fig. 11: Cross-sectional area of the MHP.

The section is symmetric about the vertical and horizontal axes. The section has a side length, s , and each vertex has an angle of 60 degrees.

Several relationships were noted. As the size and, therefore, the hydraulic diameter of the MHP increased, each MHP was capable of dissipating more heat. However, increasing the size limited the number of MHPs the spreader could accommodate, thereby reducing the total power that could be applied. The pattern radius could be increased allowing a greater number of MHPs to fit on the spreader, but doing so would limit the contact area of the evaporator to the heat source and limit the number of MHPs because of the heat capacity. After several iterations, it was determined that a pattern radius of 4.25 mm and a star side length of 1.1 mm would result in the greatest heat capacity and the greatest quantity of MHPs. These chosen parameters resulted in a maximum number of 8 MHPs that could be used.

It was found that the MHP heat capacity was largely dependant on the working temperature used to obtain the fluid properties. Based on the heat capacity equation used, at higher working temperatures the MHP was able to dissipate more heat, which affected the power input that could be applied to the spreader. The minimum surface temperature of the spreader was not allowed to fall below the working temperature of the MHP to ensure proper MHP operation. In practice, the working temperature of a heat pipe is found through detailed analysis of heat pipe operation that involves the casing material, the working fluid, the liquid charge, the inner heat pipe pressure etc. In this study, the working temperature was not allowed to exceed the maximum desired surface temperature of the spreader for all power inputs. For the purposes of this study, the maximum surface temperature could not exceed 105°C, per Rockwell Collins' specifications. The minimum surface temperature was assumed to be 30°C. Thus, the maximum and minimum working temperatures were chosen to be 100°C and 35°C, respectively. For each quantity of MHPs, the maximum power input was calculated for the maximum and minimum working temperature. The results are shown in Fig 12. At a working temperature of 35°C, the power input range was 2.1 W to 17.1 W where each MHP had a heat capacity of 2.1 W. At a working temperature of 100°C, the power input range was 22.4 W to 179.1 W where each MHP could dissipate 22.4 W.

Parametric Table		
at 35 deg		
1..10	Quantity _{MHPs}	Q _{input} [W]
Run 1	1	2.145
Run 2	2	4.29
Run 3	3	6.435
Run 4	4	8.58
Run 5	5	10.72
Run 6	6	12.87
Run 7	7	15.01
Run 8	8	17.16
Run 9		
Run 10		

Parametric Table		
at 100 deg		
1..10	Quantity _{MHPs}	Q _{input} [W]
Run 1	1	22.39
Run 2	2	44.78
Run 3	3	67.17
Run 4	4	89.56
Run 5	5	112
Run 6	6	134.3
Run 7	7	156.7
Run 8	8	179.1
Run 9		
Run 10		

Fig. 12: Power inputs as a function of the quantity of MHPs.
Shown at working temperatures of 35°C (left) and 100°C (right).

5.1.2 MECHANICA

Each array configuration, from two equally spaced MHPs to eight equally spaced MHPs, was modeled in MECHANICA. All array configurations are shown in the Array Configuration section in the Appendix. The MHPs were patterned with equal angle spacing between each MHP about the pattern radius. For example, an array with 2 MHPs had MHPs that were 180 degrees apart, an array with 3 MHPs had MHPs that were 120 degrees apart and so on. Each MHP consisted of three equal sections where the middle section had an adiabatic surface. Finding the optimal lengths for each section would require an in-depth analysis of the MHP physics, which was beyond the scope of this research. Therefore, equal lengths for each section was chosen. It should be noted that

these lengths do affect the results. For example, if the adiabatic section was too long, there would be more heat transferred to the end of the MHP, thereby overestimating the spreading resistance. For each configuration three different MHP effective thermal conductivities of 5,000 W/m°C, 50,000 W/m°C, and 100,000 W/m°C were tested for a range of power inputs. A convection boundary condition of $h=100 \text{ W/m}^2\text{°C}$ with an ambient temperature of $T_\infty=20\text{°C}$ was applied to the base of the copper spreader on the opposite side of the heat source. All surfaces except the heat source area where the power was applied and the base where the convection condition was applied, were adiabatic.

The heat source area was divided into four equal areas. For each area a temperature measure was placed in the center. A temperature measure is used at a point on the model where the temperature is to be measured. The base of the spreader was divided into 16 equal areas where 16 temperature measures were placed in the center. The location of where the temperatures were measured is shown in Fig. 13. Temperatures 01 to 04 were contained on the top surface of the spreader within the heat source area and temperatures 05 to 20 were located on the base of the spreader opposite the side of the heat source. Temperatures 01 to 04 were averaged to find the average source temperature, and temperatures 05 to 20 were averaged to find the average base temperature. Then using Equations 10 and 11, the average and maximum spreading resistances were calculated.

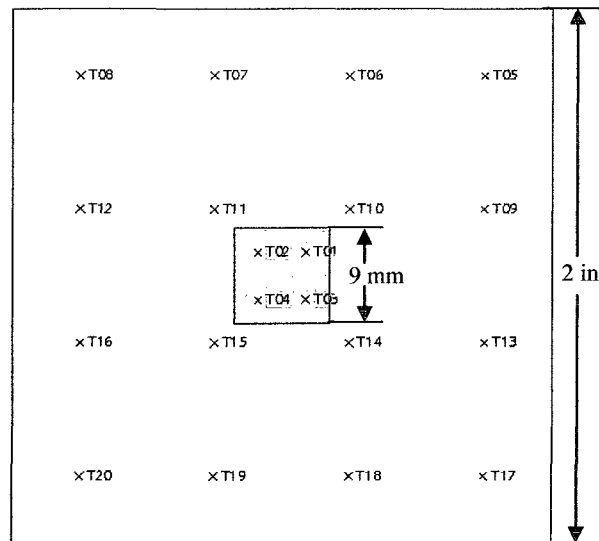


Fig. 13: Temperature measures.

Copper spreader with applied heat load area showing where the temperatures are measured in MECHANICA . Temperatures 1-4 are on the heat source surface whereas temperatures 5-20 are on the bottom surface of the base of the spreader.

For one array, the convective boundary condition was varied to determine if it affected the spreading resistance. Also for one array, the effective thermal conductivity of the MHP was varied to examine how it affected the spreading resistance

When using EES, the heat capacity of the MHPs was calculated as explained in the previous section. This, in turn, revealed the number of MHPs that could be used in the study, as well as what power range was acceptable such that the heat capacity of the MHP was not violated. However, the calculations did not factor in the spreader material, the MHP configuration, the boundary conditions, or the application in general.

Therefore, a preliminary MECHANICA study was conducted to determine the range of input power values appropriate for the current application. For a convection boundary condition of $h=100 \text{ W/m}^2\text{°C}$ and an ambient temperature of $T_{\infty}=20\text{°C}$ the maximum and

minimum surface temperatures were found. It was expected that the minimum surface temperature would occur at the lower end of the power range at the largest value of k_{eff} of 100,000 W/m²°C and the greatest number of MHPs of eight. Input powers of 1 W to 5 W were simulated and the resultant temperatures were examined. It was found that a power input less than 3 W resulted in surface temperatures less than 30°C. Therefore, 3 W was the minimum power that was simulated for the remainder of this study. The maximum surface temperature was expected to occur at the higher end of the power range at the lowest k_{eff} of 5,000 W/m²°C and at an array configuration of two MHPs. For this case, input powers ranging from 19 W to 25 W were simulated because these power inputs resulted in the range of surface temperatures that needed to be examined, which was around 105 °C. It was found that surface temperatures exceeded 105°C when the power input was greater than 21 W. Therefore, 21 W was the maximum value of input power that was simulated for the rest of the study. The 45 W that was originally thought to be tested no longer applied because of the MHP limitations. It should be noted that the MHPs reached their heat capacity limitation where the power was greater than the allowed value found from the EES calculations, which were shown in Fig 12. For example, for an operating temperature of 35°C the maximum heat that 5 MHPs could effectively dissipate was 10.7 W. Any higher and the MHP may reach dryout. The actual calculations for this were beyond the scope of this study. One must be aware of the MHP limitations when examining the results and be conscientious of the fact that the working temperature (as well as other parameters) greatly affected these MHP limitations. By changing parameters such as the working fluid, geometry or convection

boundary condition, a value of 45 W may be possible. The final parameters used for the study is found in Table 2.

Table 2: Parameters defined in the MECHANICA simulations.

Initial Specifications	
Material of the spreader	Copper
Thermal conductivity for the spreader	400 W/m°C
Size of the spreader	2 in x 2 in
Area of the heat source	9 mm x 9 mm
Maximum surface temperature	105°C
Minimum surface temperature	30°C
Input Parameters	
Cross-sectional side length of the MHP, s	1.10 mm
Longitudinal length of the MHP, L	20 mm
Pattern radius, r	4.25 mm
Calculated Parameters	
Hydraulic diameter of the MHP, D_h	1.9 mm
Maximum heat capacity per MHP, Q_{max}	
at working temp of 35°C	2.14 W
at working temp of 100°C	22.4 W
Maximum number of MHPs, $Quantity_{MHPs}$	8
Chosen Parameters	
Spreader thickness	4.0 mm
MHP k_{eff} values	5,000 W/m°C, 50,000 W/m°C, and 100,000 W/m°C
Power inputs values	3W, 6W, 9W, 12W, 15W, 18W, and 21W
Convective boundary condition	100 W/m ² °C

5.2 Results and Discussion

5.2.1 Surface Temperatures and Power Input

For each array configuration, three thermal conductivities were tested. For each conductivity, power was varied from 3 W to 21 W. The temperature at each point, shown in Fig. 13, was recorded. The maximum source temperature, the average source temperature, and the average base temperature were all tabulated for each power input, shown in Table 3, along with the calculated values for the average and maximum spreading resistance. The results shown are for Array 8 with a heat transfer coefficient of $100 \text{ W/m}^2\text{°C}$ and an effective thermal conductivity of $100,000 \text{ W/m}^2\text{°C}$. A plot of the temperature results are shown in Fig. 14. The plot shows the expected result that surface temperatures increase as power increases. Due to the scale of the plot it seems the source and base temperatures are identical. This is not the case, however. The temperature values are seen easier on the table. Although small, there is a difference between the source and base temperatures. Using this temperature difference, the average and maximum spreading resistance is determined. The plot of the spreading resistance is depicted in Fig. 15. The difference between the average and maximum spreading resistance is 31.7%. From the plot it is clearly seen that spreading resistance does not change as power increases, meaning that the spreading resistance is independent of power for a constant effective thermal conductivity. This trend was found to be typical for all array configurations with a constant conductivity. This was expected after examining the spreading resistance formulas seen in Equations 1 through 9. None of the equations show that the spreading resistance is a function of power input. Therefore, instead of plotting

the spreading resistance with respect to power, it should be examined with respect to the effective thermal conductivity of the MHP. The effective thermal conductivity with respect to the power input is shown in the next section.

Table 3: Temperature and spreading resistance.

Results are for Array 8, $h=100 \text{ W/m}^2\text{°C}$ and $k_{\text{eff}}=100,000 \text{ W/m}^2\text{°C}$.

	$k_{\text{eff}}=100,000 \text{ W/m}^2\text{°C}$						
Power Input:	3W	6W	9W	12W	15W	18W	W
Max Temp [°C]:	31.878	43.756	55.634	67.512	79.391	91.269	103.147
Source Avg [°C]:	31.798	43.595	55.393	67.190	78.988	90.785	102.583
Base Avg [°C]:	31.624	43.247	54.871	66.494	78.118	89.741	101.365
R_{avg} [°C/W]:	0.058	0.058	0.058	0.058	0.058	0.058	0.058
R_{max} [°C/W]:	0.085	0.085	0.085	0.085	0.085	0.085	0.085

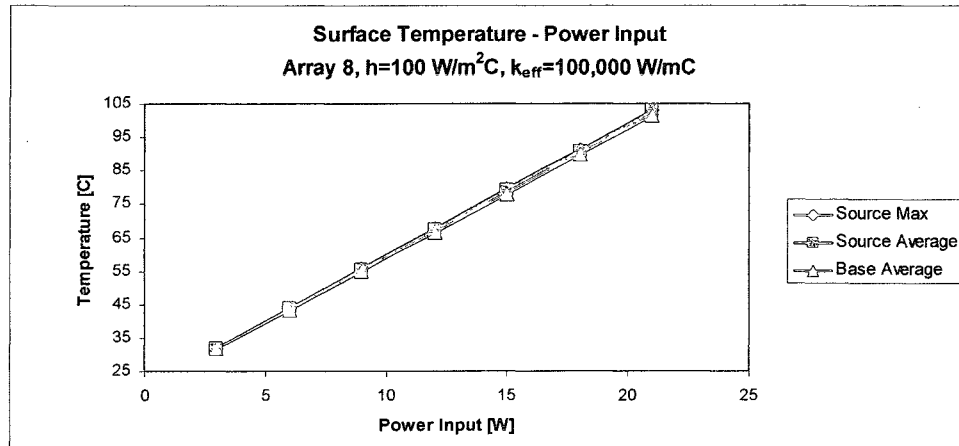


Fig. 14: Surface temperatures as a function of power input.
The temperatures increase linearly with respect to power.

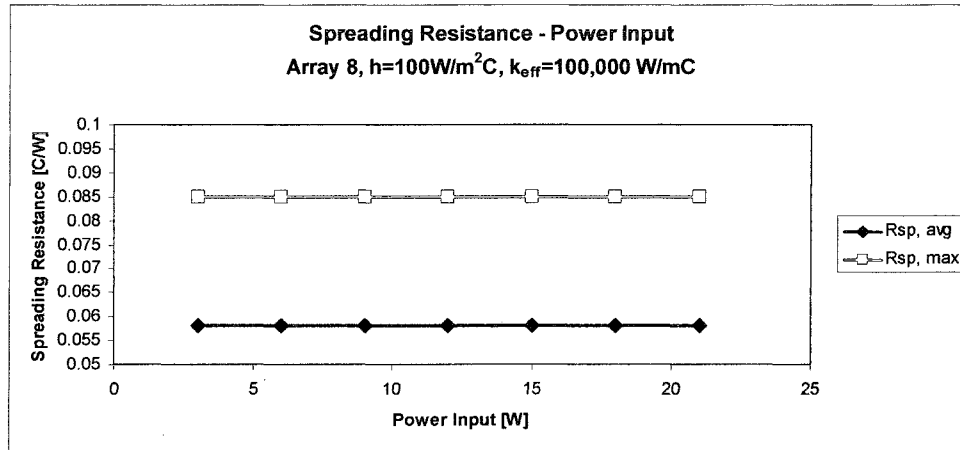


Fig. 15: Average and maximum spreading resistance as a function of power.
 Spreading resistance is constant over all power inputs.

5.2.2 Array Configuration and Effective Thermal Conductivity

For each array, the average and maximum spreading resistance as a function of the number of MHPs in the array was simulated for each effective thermal conductivity. The resultant plots are shown in Fig. 16.

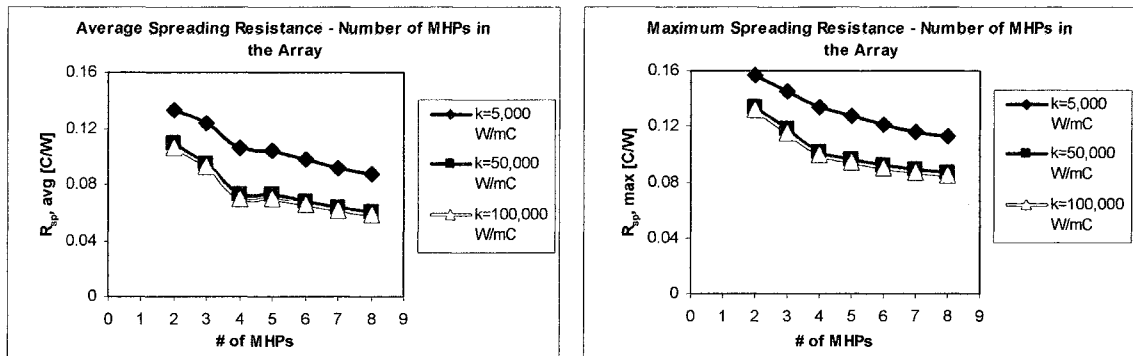


Fig. 16: Average and maximum spreading resistance as function of the quantity of MHPs.

The plot is shown for three different conductivities.

Both plots have the same scale and are placed next to each other so that the difference between the average and maximum spreading resistance are easily compared. Both plots show a similar trend with respect to the number of MHPs, but the maximum spreading resistance is shifted up by approximately 18.2%. For each conductivity the spreading resistance decreases as the number of MHPs increases. Due to the limitations for the star shaped MHP, arrays consisting of more than eight MHPs are not studied. Nonetheless, as the number of MHPs goes beyond eight, it is expected that the spreading resistance will continue to drop until it levels off at a certain value. It is shown from the plot that the slope changes considerably between two to four MHPs and four to eight MHPs. It is expected to decrease further until reaching a value close to zero. When this occurs, it would reveal the maximum number of MHPs and the minimum spreading resistance that can be achieved. As long as the size of the heat source and spreader are the same, this minimum value of spreading resistance will be constant for all values of power input, according to the previous discussion.

The spreading resistances were also plotted as a function of the conductivity tested for each array configuration. The plot is shown in Fig. 17. The same information is conveyed in Fig. 17 as in Fig. 16, but with the dependant variable changed. From this plot, it's also easily seen that both the average and maximum spreading resistance decreases as the number of MHPs increases. Table 4 shows the decrease in spreading resistance for each thermal conductivity when the number of MHPs is increased from two to eight. The greatest decrease occurs at the highest conductivity of $100,000 \text{ W/m}^{\circ}\text{C}$,

where the average spreading resistance decreases by 45.4%, and the maximum spreading resistance decreases by 35.7% as the number of MHPs increases from two to eight.

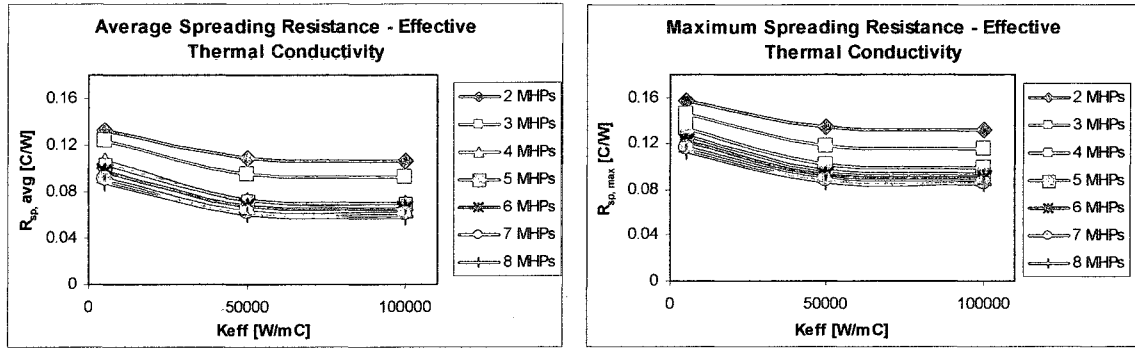


Fig. 17: Average and maximum spreading resistance as a function of effective thermal conductivity.

Table 4: Spreading resistance percent decrease from 2 MHPs to 8 MHPs.

	Average Spreading Resistance			Average Spreading Resistance		
	2 MHPs	8 MHPs	% decrease	2 MHPs	8 MHPs	% decrease
$k=5,000$ W/m°C	0.13305	0.08712	34.5	0.15733	0.11246	28.5
$k=50,000$ W/m°C	0.1087	0.0598	45.0	0.13408	0.08665	35.4
$k=100,000$ W/m°C	0.1063	0.058	45.4	0.13184	0.0848	35.7

Figure Fig. 17 also shows an interesting trend with respect to the effective thermal conductivity. The spreading resistance starts to decrease but then becomes more or less constant between 50,000 W/m°C and 100,000 W/m°C. This leads one to believe that beyond 50,000 W/m°C, the effective thermal conductivity can no longer lead to a lower spreading resistance. To develop an appropriate trend between spreading resistance and

the MHP effective thermal conductivity, further investigation was required. Array 8 was used as an example and was tested for a wider range of conductivities. The array was tested from 400 W/m°C to 200,000 W/m°C. The results are presented in Fig. 18.

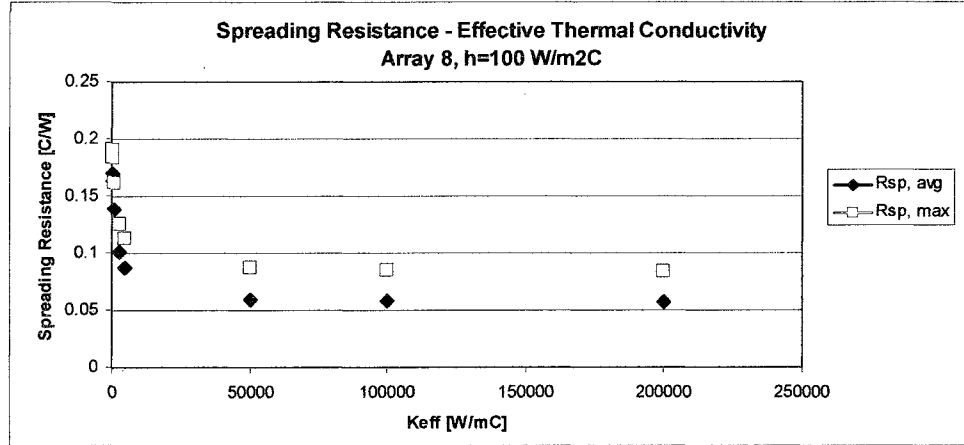


Fig. 18: Average and maximum spreading resistance for a range of effective thermal conductivities.

Spreading resistance is shown to level off at a conductivity of around 50,000 W/m°C.

At lower conductivities the spreading resistance decreases sharply. However, once the spreading resistance reaches approximately 50,000 W/m°C, it levels off. This trend shows that once this conductivity is reached, increasing the effective thermal conductivity no longer affects the spreading resistance. From the trends shown in Fig. 17, and in comparing them to this particular study, it seems that these results are typical for all array configurations. Therefore, when designing a MHP with similar specifications as in this research, the components of the MHP, such as the working fluid type and liquid charge, should be chosen such that the effective thermal conductivity results in a value of around 50,000 W/m°C, assuming a similar MHP is used. As long as the effective thermal conductivity is at least 50,000 W/m°C, the exact value is not significant.

5.2.3 Convection Boundary Condition

A convection boundary condition analysis was conducted to determine the effect the heat transfer coefficient had on the average and maximum spreading resistance. This analysis was carried out for Array 8 which had 8 MHPs spaced 45 degrees apart. Heat transfer coefficients of 10 W/m²°C, 100 W/m²°C and 1000 W/m²°C were analyzed at a bulk temperature of 20°C. These coefficient values were simulated for thermal conductivities of 5,000 W/m°C, 50,000 W/m°C, and 100,000 W/m°C. The results are shown in Fig. 19. The plot shows that the spreading resistance is rather constant, with only a maximum of a 5% increase from $h=10$ W/m²°C to $h=100$ W/m²°C. This means that the spreading resistance is independent of the boundary conditions applied for this application. The 100 W/m²°C that was used for all simulations was valid because it was representative of all boundary conditions. The boundary conditions did not have a significant effect on the spreading resistance. When inputting different convection coefficient values in the spreading resistance Equations 1 through 9, the spreading resistance value did not change significantly, showing agreement between the results from MECHANICA and theory. The MECHANICA results were also confirmed when examining Figure 7 in Ellison's paper, "Maximum Thermal Spreading Resistance for Rectangular Sources and Plates With Nonunity Aspect Ratios." In that particular figure, it was shown that there was little or no difference in the convective boundary condition for the tau value of 0.4 which was representative of the this application.

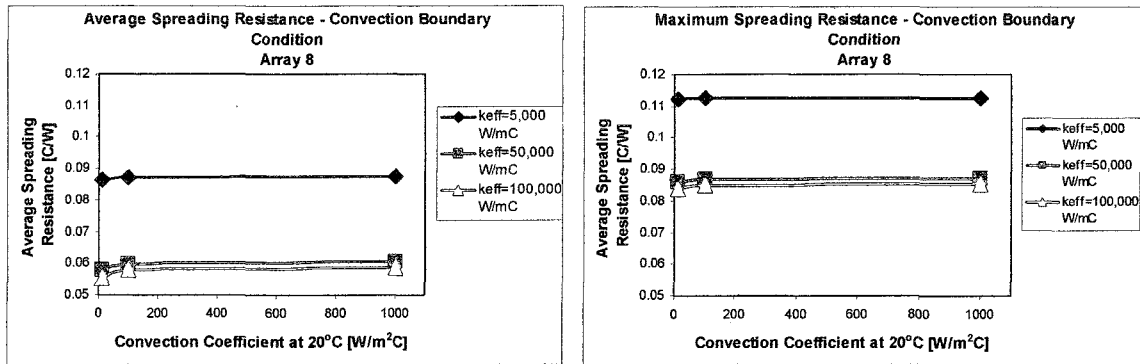


Fig. 19: Average and maximum spreading resistance.

The average (left) and maximum (right) spreading resistance as a function of the heat transfer coefficient for each effective thermal conductivity.

5.2.4 Pattern Radius

A study was conducted on one array to briefly examine the affect the pattern radius had on the spreading resistance. The study was carried out for an array containing four MHPs, one with the original pattern radius of 4.25 mm and one with a radius of 1.66 mm, such that more of the MHP end was within the heat source area as shown in Fig. 20. The simulation was performed for a convection coefficient of 100 W/m²°C and an effective thermal conductivity of 100,000 W/m°C. From the results presented in Table 5, it was shown that the array with the smaller pattern radius had a much lower spreading resistance. Decreasing the radius by 2.59 mm decreased the average spreading results by 66.6% and the maximum spreading resistance by 45.6%, showing that the pattern radius can significantly affect the spreading resistance value.

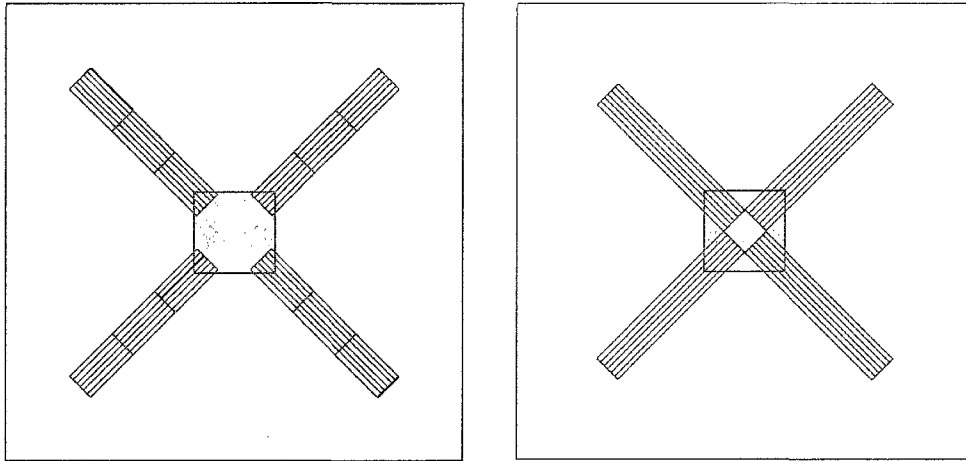


Fig. 20: Pattern radius.

Array 4 with a pattern radius of 4.25 mm (left) and 1.66 mm (right). A smaller pattern radius allows greater contact within the heat source area.

Table 5: Results of pattern radius for Array 4 at $h=100\text{W/m}^2\text{°C}$ and $k_{\text{eff}}=100,000\text{W/m}^2\text{°C}$.

	$r=4.25\text{ mm}$	$r=1.66\text{ mm}$	Percent Decrease
$R_{\text{sp, avg}}$	0.0695	0.0232	66.6%
$R_{\text{sp, max}}$	0.0991	0.0539	45.6%

5.2.5 Diamond Heat Spreader

MHP Array 8 was compared to three types of diamond spreaders: 1) a sintered polycrystalline diamond with thermal conductivities ranging from $300\text{ W/m}^2\text{°C}$ to $700\text{ W/m}^2\text{°C}$, 2) a polycrystalline diamond made from a low pressure CVD process with thermal conductivities ranging from $500\text{ W/m}^2\text{°C}$ to $1300\text{ W/m}^2\text{°C}$, and 3) a single crystal diamond made from a high pressure CVD process with thermal conductivities ranging

from 1500 W/m°C to 2100 W/m°C (Rogacs and Rhee). The low and high ends of the thermal conductivities were simulated for each type of diamond with a convection coefficient of 100 W/m²°C. The maximum and average spreading resistance was calculated and is shown in Fig. 21 in comparison with the MHP array. The MHP array had 8 MHPs in a radial configuration with an effective thermal conductivity of 100,000 W/m°C. These MHPs were embedded in a copper spreader where $k=400$ W/m°C.

For the sintered polycrystalline diamond, both the average and maximum spreading resistances were greater than that of the MHP array suggesting that using MHPs instead of a sintered polycrystalline diamond would be more effective at decreasing the spreading resistance. For the CVD polycrystalline diamond, the use of MHPs on a copper spreader only improved performance if the diamond was at the lower thermal conductivity range close to 500 W/m°C. It was found that an array of eight MHPs would not be sufficient at decreasing the spreading resistance when compared to the single crystal diamond. However, from the trends presented earlier of spreading resistance as a function of the number of MHPs, if the number of MHPs was increased the spreading resistance would drop further. It was expected that the spreading resistance would level off at some point such that additional MHPs would not cause significant changes. Whether this leveling off point is greater or less than the spreading resistance of the single crystal diamond is currently unknown. Therefore, the thermal performance of an array with greater than eight MHPs could not be accurately compared to the single crystal diamond.

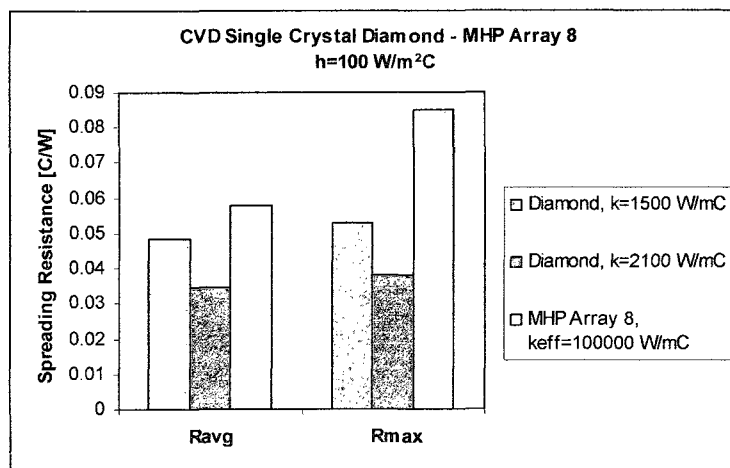
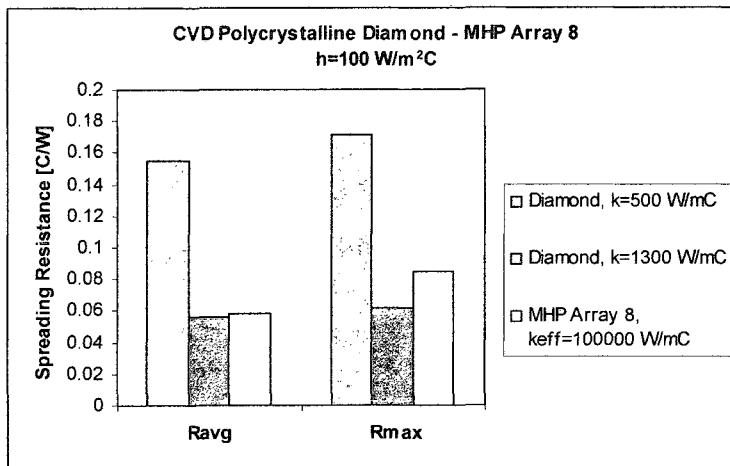
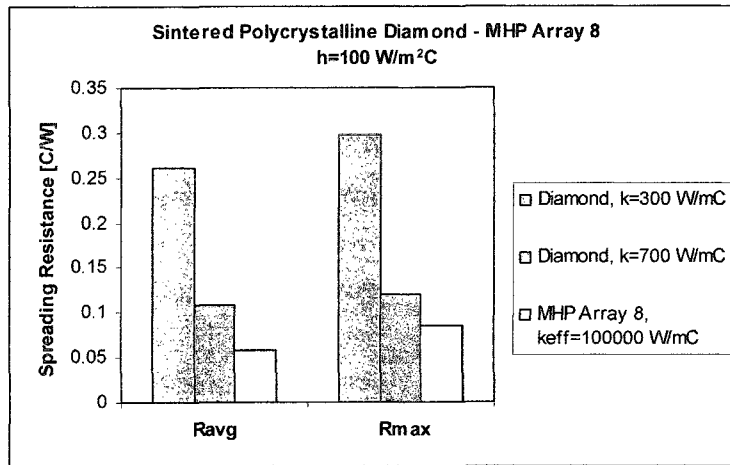


Fig. 21: Spreading resistance of three different types of diamond spreaders, all compared to MHP Array 8.

6 Conclusions and Recommendations

The spreading resistance of a 9 mm by 9 mm heat source applied to a 2 inch by 2 inch spreader was reduced by implementing MHP arrays. Seven arrays, ranging from two MHPs to eight MHPs in a radial configuration were simulated using MECHANICA. Each array was tested at MHP effective thermal conductivities of 5,000 W/m²°C, 50,000 W/m²°C, and 100,000 W/m²°C, and for a range of power inputs from 3 W to 21 W.

Several trends were observed. For a constant thermal conductivity, the surface temperatures of the spreader increased as the power input increased. The relationship was linear with a slope of approximately 3.96 °C/W for the maximum source temperature, 3.93 °C/W for the average source temperature, and 3.87 °C/W for the average base temperature. Although the surface temperature increased with power input, the spreading resistance remained constant, indicating that the spreading resistance was independent of power as expected from the spreading resistance theory. It was also shown that the spreading resistance was independent of the convection coefficient. At values of 10 W/m²°C, 100 W/m²°C, and 1,000 W/m²°C, the spreading resistance value remained fairly constant. The spreading resistance decreased, however, when the MHP effective thermal conductivities and number of MHPs were increased. It was found that once a thermal conductivity of around 50,000 W/m²°C was achieved, the spreading resistance reached its limit and no longer changed significantly. The spreading resistance did not level off as the number of MHPs were increased. However, there was a noticeable decrease in slope suggesting that if additional MHPs were added, the

spreading resistance would eventually settle until reaching a final value where it would remain constant.

By adding embedded MHPs on a heat spreader, the spreading resistance can be reduced dramatically. From Table 6, it is shown that for a MHP thermal conductivity of 100,000 W/m°C and a convection coefficient of 100 W/m²°C, the average spreading resistance is lowered by over 70% just by adding eight MHPs, and can very well decrease further when adding additional MHPs.

Table 6: Spreading resistance comparison between no MHPs and with an array of 8 MHPs.

	No MHPs	With MHPs (Array 8, h=100 W/m ² °C, k=100,000 W/m°C)	Percent Decrease
Rsp, avg	0.1964	0.0580	70.5%
Rsp, max	0.2241	0.0848	62.1%

However, one cannot just blindly add more MHPs by decreasing the hydraulic diameter. One must be aware of all the limitations involved in designing a MHP, most importantly the boiling and capillary limits. The study presented here used a simplified heat capacity equation and by no means should be the only resource when designing a MHP for a specific application. A range of thermal conductivities and power inputs were examined because the actual calculations of these parameters were beyond the scope of this research. The best and most important way to improve the results is to examine, in detail, the physics and dynamics of MHP operation. By doing so, an accurate effective thermal conductivity can be found. Because the conductivity was strongly dependant on the

power input, it has to be re-evaluated to match the simulation parameters, such as the number of MHPs and the input power, thus giving more accurate trends specific to the particular application.

There are additional points that may need to be acknowledged when setting up MHP simulations. It is suggested to try to design a MHP small enough such that a much greater quantity can be used on the spreader geometry specified. This would result in a more useful trend when analyzing the spreading resistance as a function of the number of MHPs. With more MHPs, it would be easier to find the minimum spreading resistance that can be attained.

In the current research, the MHPs were patterned around the heat source with a 4.25 mm radius so that a greater quantity of MHPs could be analyzed. It is suggested to try to decrease the radius such that more or all of the evaporator portion of the MHP is within the heat source area. This, in turn, would allow the MHP to be longer so that a greater area is covered, and the heat is spread more effectively. It may also be useful to not consider a pattern radius at all but instead position the MHP such that the same area is within the heat source for each MHP. Consider Array 3 shown in Fig. 22. It is shown, because of a circular pattern radius on a square heat source, that the two lower MHPs contact more of the heat source area than the top MHP. Adjusting the way the MHPs are positioned can not only increase the contact area but it would spread the heat more evenly, providing a lower spreading resistance. Another option is to use curved MHPs to create a larger contact area between the MHP and the heat source. This allows the

evaporator section to be longer which, in turn, provides greater heat capacity per MHP, resulting in a lower spreading resistance.

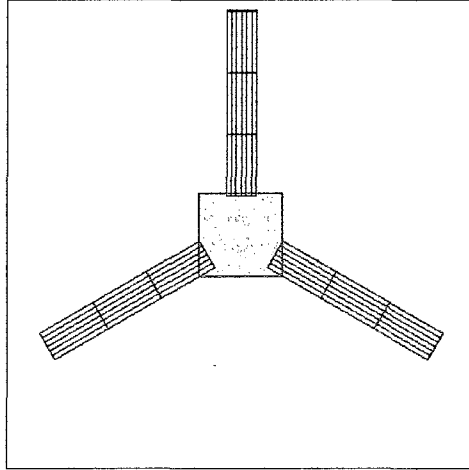


Fig. 22: Array 3 patterned around the heat source with a radius of 4.25 mm.
The two lower MHPs contact more of the heat source area than the top MHP.

In conclusion, embedding MHPs on a spreader can dramatically reduce the spreading resistance and provides more effective cooling. The current research gives a general idea of how spreading resistance is affected by various parameters, such as boundary conditions, MHP quantity, and effective thermal conductivity. This research will prove to be a useful guide for implementing similar procedures in acquiring spreading resistance trends specific to a particular application.

Works Cited

- Babin, B.R., G.P. Peterson and D. Wu. "Steady-State Modeling and Testing of a Micro Heat Pipe." *Journal of Heat Transfer* 112.3 (1990): 595-601. *Engineering Village* 2. Web. 5 April 2009.
- Cao, Yiding and Amir Faghri. "Micro/Miniature Heat Pipes and Operating Limitations." *Enhanced Heat Transfer* 1.3 (1994): 265-74. *ILLIAD*. Web. 14 Oct. 2008.
- Cao, Y., M. Gao, J.E. Beam and B. Donovan. "Experiments and Analysis of Flat Miniature Heat Pipes." *IEEE* (1996): 1402-09. *Engineering Village* 2. Web. 5 April 2009.
- Cotter, T.P. "Principles and Prospects of Micro Heat Pipes." *Proceedings of the 5th International Heat Pipe Conference* Tsukuba, Japan (1984): 328-35.
- Ellison, Gordon N. "Maximum Thermal Spreading Resistance for Rectangular Sources and Plates With Nonunity Aspect Ratios" *IEEE Transactions on Components and Packaging Technologies* 26.2 (2003): 439-54. *Engineering Village* 2. Web. 5 April 2009.
- Faghri, Amir. *Heat Pipe Science and Technology*. Washington D.C.: Taylor and Francis, 1995.
- Ha, J.M. and G.P. Peterson. "The Heat Transport Capacity of Micro Heat Pipes." *Journal of Heat Transfer* 120.4 (1998): 1064-71. *Engineering Village* 2. Web. 5 April 2009.
- Kang, Shung-Wen and Derlin Huang. "Fabrication of Star Grooves and Rhombus Grooves Micro Heat Pipe." *Journal of Micromechanics and Microengineering* 12 (2002): 525-31. *Engineering Village* 2. Web. 5 April 2009.
- Lee, Seri, Seaho Song, Van Au and Kevin P. Moran. "Constriction and Spreading Resistance Model for Electronics Packaging." *ASME/JSME Thermal Engineering Conference* 4 (1995): 199-206. *ILLIAD*. Web. 18 Sep 2008.
- Mallik, A.K., G.P. Peterson and M.H. Weichold. "On the Use of Micro Heat Pipes as an Integral Part of Semiconductor Devices." *Journal of Electronic Packaging* 114.4 (1992): 436-42. *Engineering Village* 2. Web. 5 April 2009.
- McCloskey, Alan. "How does a Heat Pipe Work? Heat Pipes Explained." OCMoDShop. 15 Aug. 2007. Web. 14 Sep. 2008 <<http://www.ocmodshop.com/ocmodshop.aspx?a=920>>

- Okamoto, Nicole, Jinny Rhee, John Lee and Stacy Gleixner. "Cost-Effective Solutions for Overcoming Conduction Spreading Resistance." Prepared for Rockwell-Collins International. San Jose State University, San Jose. 24 Apr. 2008. Reading.
- Okamoto, Nicole. Personal interview. 8 Sep. 2008.
- Peterson, G.P., A.B. Duncan and M.H. Weichold. "Experimental Investigation of Micro Heat Pipes Fabricated in Silicon Wafers." *Journal of Heat Transfer* 115.3 (1993): 751-56. *ILLIAD*. Web. 9 Oct. 2008.
- Rogacs, Anita and Jinny Rhee. "Performance-Cost Optimization of a Diamond Heat Spreader." *12th IEEE International Symposium on Advanced Packaging Materials: Processes, Properties and Interfaces, 03-05 October 2007*. Institute of Electrical and Electronics Engineers Inc. (2008). 65-72. *Engineering Village 2*. Web. 5 April 2009.
- Sobhan, C.B. and G.P. Peterson. "Modeling of the Flow and Heat Transfer in Micro Heat Pipes." *Proceedings of the 2nd International Conference on Microchannels and Minichannels 17-19 June 2004*. Rochester Institute of Technology (2004). 883-890. *ILLIAD*. Web. 16 Oct. 2008.
- Song, Seaho, Seri Lee and Van Au. "Closed-Form Equation for Thermal Constriction/Spreading Resistances with Variable Resistance Boundary Condition." *Proceedings of the 1994 International Electronics Packaging Conference, Atlanta, Georgia (1994)*: 111-21. *Engineering Village 2*. Web. 5 April 2009.
- Suman, Balram, Sirshendu De and Sunando DasGupta. "A Model of the Capillary Limit of a Micro Heat Pipe and Prediction of the Dry-Out Length." *International Journal of Heat and Fluid Flow* 26.3 (2004): 495-505. *Engineering Village 2*. Web. 5 April 2009.
- Thyrum, Geoffery and Ellen Cruse. *A Simplified Technique for Modeling Heat Pipe Assisted Heat Sinks*. Advanced Packaging. Dec. 2001. Web. 14 Sep. 2008
<http://ap.pennnet.com/display_article/129170/36/ARTCL/none/none/1/Heat-pipe-simulation/>
- Yeh, Lian-Tuu and Richard C. Chu. *Thermal Management of Microelectronic Equipment: Heat Transfer Theory, Analysis Methods, and Design Practices*. New York: ASME Press, 2002.

Appendix

EES Formula Sheet

"Assume all triangles are the same size. Each triangle has the same angle of 60 degrees. Calculate D_h"

s=.001100 [m]

b_tri=s

h_tri=sqrt(s^2-(s/2)^2)

A_tri=0.5*(b_tri*h_tri)

A_star=12*A_tri

P_star=s*12

D_h=4*A_star/P_star

"Calculate total height and width of the star"

h_star=4*h_tri

w_star=3*s

"Max number of MHPs that can be used given the spreader geometry"

r=.004250

C=2*PI*r

MaxNumber=C/w_star

"Calculate max power for each MHP and minimum # of MHPs required"

T_working= 100[C]

Q_input=3 [W]

L= .020 [m]

sigma= surfacetension(water, T=T_working)

h_fg= 2257000 [J/kg]

mu_v=viscosity(Water,x=1,T=T_working)

vol=Volume(Water,x=1,T=T_working)

v_v=mu_v*vol

Q_max=0.01*((sigma*h_fg*D_h^3)/(v_v*L))

Quantity_MHPs=Q_input/Q_max

{Q_max= maximum heat transport rate per MHP, W

sigma= liquid surface tension, N/m

h_fg= latent heat of evaporation, 2257000 J/kg

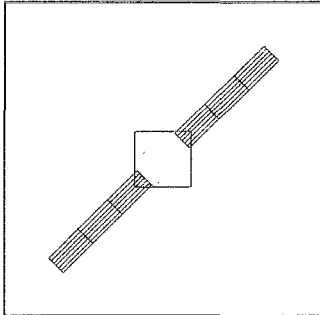
D_h= hydraulic diameter, m

v_v= vapor kinematic viscosity, m^2/s

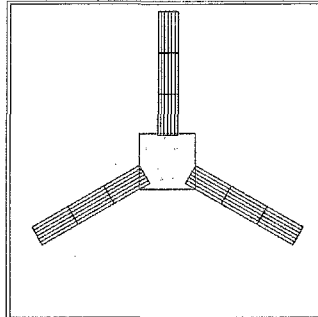
L= total length of the heat pipe, m}

Array Configurations

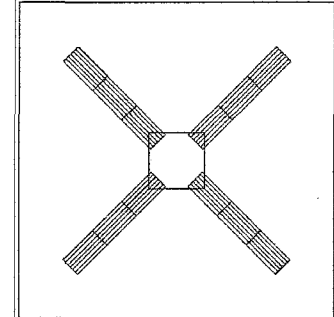
Array 2



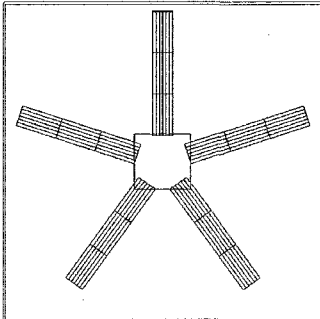
Array 3



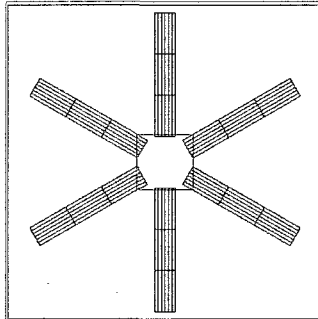
Array 4



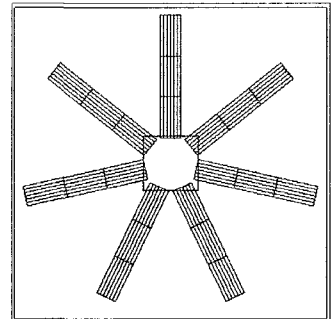
Array 5



Array 6



Array 7



Array 8

